APPROVED FOR PUBLIC RELEASE, DISTRIBUTION UNLIMITED

TI-ALEX(01)-TR-77-05

12 B.S.

STUDY OF ADAPTIVE BEAMFORMING ALGORITHMS FOR LOW MAGNITUDE SEISMIC P-WAVE DETECTION

TECHNICAL REPORT NO. 5

VELA NETWORK EVALUATION AND AUTOMATIC PROCESSING RESEARCH

Prepared by
Wen-Wu Shen

TEXAS INSTRUMENTS INCORPORATED
Equipment Group
Post Office Box 6015
Dallas, Texas 75222

AD A050317

AD No.
DDC FILE COPY

DDC
RECEIVED
FEB 23 1978
F

Prepared for

AIR FORCE TECHNICAL APPLICATIONS CENTER
Alexandria, Virginia 22314

Sponsored by

ADVANCED RESEARCH PROJECTS AGENCY
Nuclear Monitoring Research Office
ARPA Program Code No. 7F10
ARPA Order No. 2551

1 November 1977

Acknowledgment: This research was supported by the Advanced Research Projects Agency, Nuclear Monitoring Research Office, under Project VELA-UNIFORM, and accomplished under the technical direction of the Air Force Technical Applications Center under Contract Number F08606-77-C-0004.

APPROVED FOR PUBLIC RELEASE, DISTRIBUTION UNLIMITED

(14) TI-ALEX(81)-TR-77-85

(12)

(6) STUDY OF ADAPTIVE BEAMFORMING ALGORITHMS FOR LOW MAGNITUDE SEISMIC P-WAVE DETECTION,

(9) TECHNICAL REPORT NO. 5

VELA NETWORK EVALUATION AND AUTOMATIC PROCESSING RESEARCH

Prepared by

(10) Wen-Wu Shen

TEXAS INSTRUMENTS INCORPORATED
Equipment Group
Post Office Box 6015
Dallas, Texas 75222

DDC
FEB 23 1978
F

(15) F08606-77-C-0004
ARPA Order-2551

Prepared for

AIR FORCE TECHNICAL APPLICATIONS CENTER
Alexandria, Virginia 22314

Sponsored by

ADVANCED RESEARCH PROJECTS AGENCY
Nuclear Monitoring Research Office
ARPA Program Code No. 7F10
ARPA Order No. 2551

(11) 1 Nov 77 (12) 60P.

Acknowledgment: This research was supported by the Advanced Research Projects Agency, Nuclear Monitoring Research Office, under Project VELA-UNIFORM, and accomplished under the technical direction of the Air Force Technical Applications Center under Contract Number F08606-77-C-0004.

405 076 JOB

UNCLASSIFIED

SECURITY CLASSIFICATION OF THIS PAGE (When Data Entered)

REPORT DOCUMENTATION PAGE		READ INSTRUCTIONS BEFORE COMPLETING FORM
1. REPORT NUMBER	2. GOVT ACCESSION NO.	3. RECIPIENT'S CATALOG NUMBER
4. TITLE (and Subtitle) STUDY OF ADAPTIVE BEAMFORMING ALGORITHMS FOR LOW MAGNITUDE SEISMIC P-WAVE DETECTION		5. TYPE OF REPORT & PERIOD COVERED Technical 6. PERFORMING ORG. REPORT NUMBER ALEX(01)-TR-77-05
7. AUTHOR(s) Wen-Wu Shen		8. CONTRACT OR GRANT NUMBER(s) F08606-77-C-0004
9. PERFORMING ORGANIZATION NAME AND ADDRESS Texas Instruments Incorporated Equipment Group Dallas, Texas 75222		10. PROGRAM ELEMENT, PROJECT, TASK AREA & WORK UNIT NUMBERS VELA T/7705/B/ETR
11. CONTROLLING OFFICE NAME AND ADDRESS Advanced Research Projects Agency 1400 Wilson Boulevard Arlington, Virginia 22209		12. REPORT DATE 1 November 1977 13. NUMBER OF PAGES 58
14. MONITORING AGENCY NAME & ADDRESS(if different from Controlling Office) Air Force Technical Applications Center VELA Seismological Center Alexandria, Virginia 22314		15. SECURITY CLASS. (of this report) UNCLASSIFIED 15a. DECLASSIFICATION/DOWNGRADING SCHEDULE

16. DISTRIBUTION STATEMENT (of this Report)

APPROVED FOR PUBLIC RELEASE, DISTRIBUTION UNLIMITED

17. DISTRIBUTION STATEMENT (of the abstract entered in Block 20, if different from Report)

18. SUPPLEMENTARY NOTES

ARPA Order No. 2551

19. KEY WORDS (Continue on reverse side if necessary and identify by block number)

Adaptive Beamformer
Minimum Power
Short-Period Array
Time-Varying Adaptation Rate
Levins Filter Weight Constraints
Korean Seismic Research Station

20. ABSTRACT (Continue on reverse side if necessary and identify by block number)

A linear adaptive algorithm was developed for array beamforming purposes. The design goal for the algorithm was to minimize the squared filter output subject to the constraint which allows energy propagating from the array steering direction to pass without being distorted. The adaptive filter coefficients were designed as time-varying filters applied to each channel subject to the above constraints. The adaptation rate was inversely → next page

DD FORM 1 JAN 73 1473 EDITION OF 1 NOV 65 IS OBSOLETE

UNCLASSIFIED

SECURITY CLASSIFICATION OF THIS PAGE (When Data Entered)

20. continued

cont → varied with filter output and total input channel power. Performance of the algorithm was studied by using recorded short-period array data from the Korean Seismic Research Station. To demonstrate adaptive beamforming, a high amplitude signal from Kamchatka, a medium amplitude signal from eastern Kazakh, and a number of low amplitude signals from central Eurasia were processed. Results of signal-to-noise ratio gain relative to a conventional beamformer among the events tested were consistent and were in the range of 4.5 to 6.5 dB in the wide passband. Much better signal-to-noise ratio improvement was obtained in a low frequency passband.

The directivity response pattern suggested that the adaptive filter maintained a response similar to that of conventional beamforming in the 60° beamwidth of the mainlobe and was better beyond the mainlobe. Also, simulation with signal added to scaled noise at various levels suggested that the processing gain and threshold reduction were consistent.

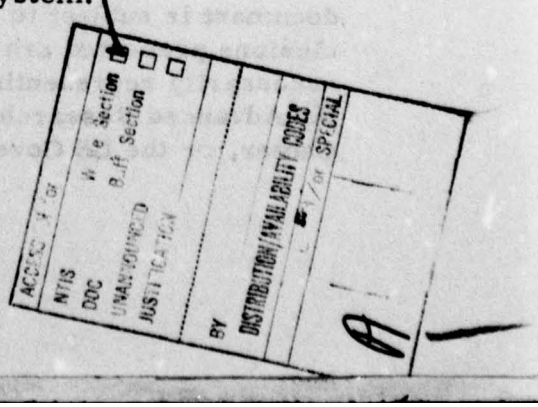
The adaptive algorithm was programmed in the real-time mode and can be implemented in a front-end system.

ABSTRACT

A linear adaptive algorithm was developed for array beamforming purposes. The design goal for the algorithm was to minimize the squared filter output subject to the constraint which allows energy propagating from the array steering direction to pass without being distorted. The adaptive filter coefficients were designed as time-varying filters applied to each channel subject to the above constraint. The adaptation rate was inversely varied with filter output and total input channel power. Performance of the algorithm was studied by using recorded short-period array data from the Korean Seismic Research Station. To demonstrate adaptive beamforming, a high amplitude signal from Kamchatka, a medium amplitude signal from eastern Kazakh, and a number of low amplitude signals from central Eurasia were processed. Results of signal-to-noise ratio gain relative to a conventional beamformer among the events tested were consistent and were in the range of 4.5 to 6.5 dB in the wide passband. Much better signal-to-noise ratio improvement was obtained in a low frequency passband.

The directivity response pattern suggested that the adaptive filter maintained a response similar to that of conventional beamforming in the 60° beamwidth of the mainlobe and was better beyond the mainlobe. Also, simulation with signal added to scaled noise at various levels suggested that the processing gain and threshold reduction were consistent.

The adaptive algorithm was programmed in the real-time mode and can be implemented in a front-end detection system.



ACKNOWLEDGMENTS

I gratefully thank Dr. Robert L. Sax for his constant concern and discussions and critical reading of this paper, and Mrs. Cherylann B. Saunders for typing the manuscript and preparing the figures. Thanks are also due to Messers. Thomas E. Barnard, Terence W. Harley, and Rudolf Unger for a number of comments on the manuscript.

Neither the Advanced Research Projects Agency nor the Air Force Technical Applications Center will be responsible for information contained herein which has been supplied by other organizations or contractors, and this document is subject to later revision as may be necessary. The views and conclusions presented are those of the authors and should not be interpreted as necessarily representing the official policies, either expressed or implied, of the Advanced Research Projects Agency, the Air Force Technical Applications Center, or the US Government.

TABLE OF CONTENTS

SECTION	TITLE	PAGE
	ABSTRACT	iii
	ACKNOWLEDGMENTS	iv
I.	INTRODUCTION	I-1
	A. GENERAL DESCRIPTION	I-1
	B. ORGANIZATION OF THE REPORT	I-2
II.	ADAPTIVE BEAMFORMING ALGORITHM	II-1
	A. MINIMUM POWER WITH LEVIN'S CONSTRAINTS	II-1
	B. TIME-VARYING ADAPTATION RATE (L_1 NORM ALGORITHM)	II-3
III.	PERFORMANCE OF THE ALGORITHM	III-1
	A. INTRODUCTORY COMMENT	III-1
	B. FULL ARRAY PERFORMANCE	III-2
	C. INNER-RING ARRAY PERFORMANCE	III-10
	D. EVALUATIONS USING LOW MAGNITUDE EVENTS	III-12
	E. RESPONSE PATTERN	III-15
	F. SIGNAL WITH SCALED NOISE SIMULATION	III-20
	G. ADAPTIVE FILTER LENGTH	III-23
IV.	CONCLUSION AND FURTHER WORK FOR IMPLEMENTATION	IV-1
	A. CONCLUSION	IV-1
	B. FURTHER WORK FOR IMPLEMENTATION	IV-2

TABLE OF CONTENTS
(continued)

SECTION	TITLE	PAGE
V.	REFERENCES	V-1
	APPENDIX	A-1

LIST OF FIGURES

FIGURE	TITLE	PAGE
III-1	THE ADAPTIVE BEAMFORMING (ABF) PERFORMANCE RELATIVE TC BEAMSTEERING VERSUS ADAPTIVE CONVERGENCE RATES. THE RESULTS ARE BASED ON THE ALGORITHM IN EQUATION (II-8). SIGNAL WAS FROM EASTERN KAZAKH ON JULY 23, 1976. ADAPTIVE FILTER LENGTH WAS 31-POINT, 17 CHANNELS WERE USED FOR BEAMSTEERING, AND SINGLE-CHANNEL DATA WERE BANDPASS (0.5-3.5 Hz) FILTERED	III-3
III-2	THE ABF PERFORMANCE RELATIVE TO BEAMSTEERING VERSUS THE ADAPTIVE CONVERGENCE RATE. THE SAME SIGNAL AS IN FIGURE 1 WAS USED IN THIS FIGURE. THE RESULTS ARE BASED ON THE ADAPTIVE ALGORITHM IN EQUATION (II-9). ADAPTIVE FILTER LENGTH WAS 31-POINT AND 17 CHANNEL DATA IN (0.5-3.5 Hz) PASSBAND WERE USED FOR BEAMFORMING	III-5
III-3	PROCESSED TRACES OBTAINED FROM THE BEAMSTEER (TRACE 1) AND THE ABF (TRACE 2) PROCESSORS. THE SIGNAL WAS FROM EASTERN KAZAKH ON JULY 23, 1976. ADAPTIVE FILTER LENGTH WAS 31-POINT AND 17 CHANNEL DATA IN (0.5-3.5 Hz) PASSBAND WERE USED FOR BEAMFORMING	III-6
III-4	THE ABF PERFORMANCE RELATIVE TO BEAMSTEERING VERSUS THE ADAPTIVE CONVERGENCE RATE. THE RESULTS ARE BASED ON THE ALGORITHM IN EQUATION (II-9). ADAPTIVE FILTER LENGTH WAS 31-POINTS AND 17 CHANNELS WERE USED. THE DATA WERE IN 0.5-1.1 Hz PASSBAND	III-8
III-5	PROCESSED TRACES OF EASTERN KAZAKH EVENT OBTAINED FROM THE BEAMSTEER (TRACE 1) AND THE ABF (TRACE 2) PROCESSORS. THE DATA WERE BANDPASS (0.5-1.1 Hz) FILTERED AND 17 CHANNEL BEAMFORMED. A 31-POINT ADAPTIVE FILTER LENGTH WAS USED	III-9

LIST OF FIGURES
(continued)

FIGURE	TITLE	PAGE
III-6	SINGLE-CHANNEL DATA FOR THE EASTERN KAZAKH EVENT IN THE 0.5-1.1 Hz PASSBAND	III-11
III-7	PROCESSED TRACES OF EASTERN KAZAKH EVENT OBTAINED FROM THE BEAMSTEER (TRACE 1) AND THE ABF (TRACE 2) PROCESSORS. ONLY SIX INNER-RING CHANNELS WERE USED FOR BEAMFORMING. THE DATA WERE IN 0.5-1.1 Hz PASSBAND AND A 31-POINT ADAPTIVE LENGTH WAS USED FOR THE ABF.	III-13
III-8	PROCESSED TRACES OBTAINED FROM THE BEAMSTEER (TRACE 1) AND THE ABF (TRACES 2 AND 3) PROCESSORS. THE SIGNAL WAS FROM TIBET ON NOVEMBER 10, 1974. USED WERE THE 19 CHANNEL DATA IN THE 0.5-3.5 Hz PASSBAND AND A 31-POINT ADAPTIVE FILTER LENGTH	III-14
III-9	MEASURED DIRECTIVITY (AZIMUTH) RESPONSE PATTERN FOR THE EVENT FROM EASTERN KAZAKH	III-16
III-10	MEASURED SNR VERSUS AZIMUTH	III-17
III-11	MEASURED VELOCITY (EPICENTRAL DELTA) RESPONSE FOR THE EVENT FROM EASTERN KAZAKH	III-18
III-12	MEASURED SNR VERSUS EPICENTRAL DELTA (EVENT AZIMUTH = 304.3° AND EVENT DELTA = 36.1°)	III-19
III-13	AMPLITUDE-WISE OPERATING CHARACTERISTICS	III-21
III-14	RMS NOISE AND SIGNAL AMPLITUDE-WISE OPERATING CHARACTERISTICS	III-22
III-15	ABF PERFORMANCE FOR VARIOUS ADAPTIVE FILTER LENGTHS	III-24

LIST OF FIGURES
(continued)

FIGURE	TITLE	PAGE
A-1	PROCESSED TRACES FOR THE EVENT FROM TURKEY, NOVEMBER 5, 1974	A-2
A-2	PROCESSED TRACES FOR THE EVENT FROM KASHMIR-INDIA BORDER, NOVEMBER 16, 1974	A-3
A-3	PROCESSED TRACES FOR THE EVENT FROM IRAQ, NOVEMBER 17, 1974	A-4
A-4	PROCESSED TRACES FOR THE EVENT FROM IRAN, NOVEMBER 22, 1974	A-5
A-5	PROCESSED TRACES FOR THE EVENT FROM GREECE-ALBANIA BORDER, NOVEMBER 23, 1974	A-6
A-6	PROCESSED TRACES FOR THE EVENT FROM SOUTHERN SINKIANG, CHINA, NOVEMBER 28, 1974	A-7
A-7	PROCESSED TRACES FOR THE EVENT FROM GREECE, NOVEMBER 14, 1974	A-8
A-8	PROCESSED TRACES FOR THE EVENT FROM WESTERN IRAN, NOVEMBER 22, 1974	A-9
A-9	PROCESSED TRACES FOR THE EVENT FROM TURKEY, NOVEMBER 23, 1974	A-10
A-10	PROCESSED TRACES FOR THE EVENT FROM SOUTHERN SINKIANG, CHINA, NOVEMBER 25, 1974	A-11
A-11	PROCESSED TRACES FOR THE EVENT FROM AFGHANISTAN-USSR BORDER, NOVEMBER 13, 1974	A-12
A-12	PROCESSED TRACES FOR THE EVENT FROM GREECE, NOVEMBER 14, 1974	A-13

SECTION I
INTRODUCTION

A. GENERAL DESCRIPTION

A linear adaptive filter algorithm is described in this paper and is applied to the problem of detecting and estimating the waves propagated from a seismic source. Under the assumption of ideal wave propagation in a homogeneous earth, the signal is defined as an identical replica on all of the sensors of an array after correction for propagation delays. The noise, on the other hand, is defined operationally as any interfering component which is not identical on all of the sensors. For example, the noise may not be identical due to differing propagation delay characteristics, due to spatial amplitude variations, due to the incoherency of waves occurring on different sensors.

In time-domain adaptive filtering, there are two basic and main mathematical concepts applied (Gangi and Byun, 1976): One is the constrained (unbiased) minimum power adaptive algorithm (Burg, et al., 1967), and the other is the unconstrained minimum "error" adaptive algorithm (Widrow, 1966). The former approach minimizes the output power of the filtered data subject to constraints. These are that the filter weights summed over all of the channels are equal to a chosen prescribed value (Levin, 1964; Frost, 1972). The latter approach uses Wiener's method and minimizes the 'errors' or the differences between the 'desired output' and the actual filtered output. Subsequent works on the unconstrained adaptive algorithm included Lintz (1968), Widrow, et al. (1969), Griffiths (1969), and others. It is noted that Wiener's method requires that the desired

signal be given a-priori and be injected into the filtering system. Other forms of adaptive algorithms are reported by Booker and Ong (1971), Wang and Treitel (1971), Winkler and Schwartz (1972), and Griffiths et al. (1977).

The algorithm to be demonstrated in this report requires neither the a-priori knowledge of noise statistics nor the a-priori information of statistics of the signals to be filtered. This method applies the technique which minimizes the filter output power subject to constraints that pass waves from the look direction without being distorted. Thus, no 'desired output' or 'pilot signal' is needed in the mathematical formulation. Hence, the algorithm is feasible for real-time applications in front-end acoustic, electromagnetic, or seismic detectors designed to detect events of unknown waveform.

B. ORGANIZATION OF THE REPORT

Various attempts to develop adaptive filtering techniques for seismic array processing purposes were made. However, only the most relatively successful algorithm is presented in this report. Section II describes the development of time-varying adaption rate and constrained minimum power adaptive beamforming processor which is essentially equivalent to L_1 norm which minimizes the absolute value of filter output formulation. The performance of the algorithm is presented in Section III where a number of sub-topics is discussed, namely; full array performance, inner-ring array performance, response pattern, signal with scaled noise simulation, and adaptive filter length. Finally, conclusions and suggested further work for implementation are presented in Section IV. In addition, the weak event processing results are compiled in Appendix A.

SECTION II
ADAPTIVE BEAMFORMING ALGORITHM

A. MINIMUM POWER WITH LEVIN'S CONSTRAINTS

Let $x_i(t)$, where $i = 1, 2, \ldots, M$, be the i^{th} channel input data which have been time-aligned at time t and $a_i(j)$, where $j = -N, \ldots, -2, -1, 0, 1, 2, \ldots, +N$, be adaptive filter weights applied to the i^{th} channel data. Then, the adaptive filter output $y(t)$ at time t is the convolution of a_i with x_i on each single channel summed over the channels:

$$y(t) = \sum_{i=1}^{M} \sum_{j=-N}^{+N} a_i(j) x_i(t - j\,\Delta t) \qquad \text{(II-1)}$$

where Δt is the sampling time interval. The number of points, $2N+1$, is defined as the adaptive filter length.

It is desired to find the filter weights $a_i(j)$ which minimize the squared filter output by solving the set of equations:

$$\nabla_a y^2(t) = 0 \qquad \text{(II-2)}$$

where ∇ is the gradient operator with respect to $a_i(j)$. In order not to eliminate the target signal, we impose Levin's filter weight constraints (Levin, 1964; Claerbout, 1976), which were designed for passing a wave propagating from the desired look direction through the array without being distorted during the power-minimization process of filtering on the filter weights, so that the trivial solution no longer exists. Mathematically, the constraints state:

$$\sum_{i=1}^{M} a_i(j) = \delta_{jo} \qquad \text{(II-3)}$$

where δ_{jo} is the Kronecker delta, as

$$\delta_{jo} = 1, \text{ if } j = 0 \text{ (j is at filter output point)}$$
$$\delta_{jo} = 0, \text{ if } j \neq 0 \text{ (j is not at filter output point).} \qquad \text{(II-4)}$$

Equations (II-2) and (II-3) can be computed efficiently by Levinson's recursion (Wiggins and Robinson, 1965; Capon et al. 1967).

But, for an adaptive beamformer (ABF) designed to operate on a real-time basis, the recursive method cannot be applied (Claerbout, 1976) because it takes substantial computer time and it needs a-priori knowledge of noise. We applied Widrow's adaptive rule for time-domain iterations by use of the steepest descent method which requires that the filter weight vector move against the gradient of power. Consequently, the iteration algorithm is as follows:

$$a_i^{t+\Delta t}(j) = a_i^t(j) - \frac{\lambda(t)}{2} \nabla_a y^2(t)$$

or

$$a_i^{t+\Delta t}(j) = a_i^t(j) - \lambda(t)\, y(t)\, x_i(t - j\Delta t) \qquad \text{(II-5)}$$

where $\lambda(t)$ is the actual adaptation rate and must be positive. $\lambda(t)$ is an artificially created factor which takes the fraction of power-gradient value into the change of filter weight. Following Widrow's original formulation, we set:

$$\lambda(t) = \frac{\mu}{\sum_{i=1}^{M} \sum_{j=-N}^{N} x_i^2(t - j\Delta t)}$$

or

$$\lambda(t) = \mu/P(t) \tag{II-6}$$

where μ is called adaptive convergence rate and is an input parameter in a computer program.

The filter weights $a_i(j)$ are initialized to satisfy the constraints of equation (II-3) which are preserved by imposing:

$$\sum_{i=1}^{M} \left[a_i^t(j) - a_i^{t+\Delta t}(j) \right] = 0 \tag{II-7}$$

for each lag j on each step of iterations, while allowing the single-channel filter weight $a_i(j)$ to be changed during the iterations. To implement equation (II-7), we add the beamsteer (conventional time-aligned and averaged) output $\bar{x}(t)$ into equation (II-5), such that:

$$a_i^{t+\Delta t}(j) = a_i^t(j) + \frac{\mu y(t) \left[\bar{x}(t - j\Delta t) - x_i(t - j\Delta t) \right]}{P(t)} \tag{II-8}$$

where

$$\bar{x}(t - j\Delta t) = \frac{1}{M} \sum_{i=1}^{M} x_i(t - j\Delta t).$$

This adaptive algorithm was studied using Alaskan Long-Period Array data (Barnard and O'Brien, 1974; Shen, 1975). However, iterations using equation (II-8) at the high convergence rate were found to have severe signal degradation which practically offsets the processing gain of eliminating the undesired noise when applied to short-period data for seismic P-wave detection (Shen, 1976).

B. TIME-VARYING ADAPTATION RATE (L_1 NORM ALGORITHM)

Significant improvements both in eliminating the undesired noise and in preventing the desired signal from being degraded can be

achieved by using an 'adaptable' or 'time-variable' convergence rate, μ. It should be noted here that $\lambda(t)$ in equation (II-6) is already a time-variable parameter for a constant μ. The variation of $\lambda(t)$ is due to non-stationary unfiltered total single-channel input power $P(t)$. Further adjustment was made by dividing the power gradient term in equation (II-8) by $|y(t)|$. Physically, it was intended to have the iteration slowed down when the adaptive filter output increases. Finally, the present adaptive beamforming (ABF) algorithm is:

$$a_i^{t+\Delta t}(j) = a_i^t(j) + \frac{\mu}{|y(t)|} \cdot \frac{y(t)\left[\overline{x}(t - j\Delta t) - x_i(t - j\Delta t)\right]}{P(t)} \quad \text{(II-9)}$$

where $|y(t)|$ is exponentially averaged (decay over the past) for one second for the $\Delta t = 0.1$ second digitized data. This algorithm in its form is essentially equivalent to the formulation that minimizes the absolute value of the adaptive filter output. However, exact L_1 norm algorithm is not studied here.

SECTION III
PERFORMANCE OF THE ALGORITHM

A. INTRODUCTORY COMMENT

The algorithm was programmed in the real-time mode for the short-period array data from the Korean Seismic Research Station (KSRS). The KSRS short-period array, positioned about 110 km southwest of Seoul, Korea, consists of 19 short-period seismometers and has an aperature of about 10 km. Its configuration is essentially two rings with one sensor located at the center. Both equations (II-8) and (II-9) were examined with the same set of data. A number of seismic events were used for the performance study. First, we used a strong earthquake from Kamchatka whose signal amplitudes recorded at the KSRS were very high and very much visible on single-channel data. This event also served the purpose of checking the computer program. Second, we used one event from eastern Kazakh which was a presumed underground nuclear explosion. The second signal recorded at KSRS belonged to a medium amplitude class. Third, a number of weak events which were either very low amplitude signals or undetected in the previous study (Shen, 1976) were processed. Some signal amplitudes were just at the noise levels of the conventional beamsteer. These were clearly visible and identifiable on the ABF output beams.

Before performing the adaptive beamforming process on the array data, each channel is bandpass-filtered in order to assess processing gains within specified frequency bands, usually the expected peak spectral band of the signal. Using high convergence rates and low frequency passband, it was found that the adaptive beamforming output was contaminated

by high frequency and low amplitude underdamped ringing. To eliminate this iteration noise, the ABF outputs and the beamsteer output beams were passed through the bandpass filter again. The ABF performance is evaluated on the basis of comparing its apparent detectability of known signals to that of a beamsteer processor.

The results presented in the following are based on the processing outputs of the medium amplitude event from eastern Kazakh. They are mostly parametric studies of the performance in terms of adaptive convergence rates. Approximately one and one-half minutes of data were processed, and that allowed one minute of noise gate prior to the computed P-wave arrival. The average noise power and its RMS (root-mean-square) amplitude were computed from the noise gate. Peak-to-peak signal amplitudes were also computed from an approximate 10-second signal window for the ABF and the beamsteer output beams. And, finally, signal-to-noise ratios (SNR) were computed from the peak-to-peak signal and RMS noise amplitudes. The SNRs were used as a measure of signal detectability for the events processed.

B. FULL ARRAY PERFORMANCE

1. Wide Passband

Figure III-1 shows the ABF performance relative to beamsteering versus the adaptive convergence rates (μ) for the algorithm in equation (II-8) with the data in the 0.5 - 3.5 Hz passband. The ABF noise reduction gain is defined as the ratio of the beamsteer beam noise power to the same time window of the ABF beam noise power in decibels. The signal enhancement is defined as the ratio of peak-to-peak signal amplitude on the adaptive output to that on the corresponding beamsteer output in decibels:

$$\text{signal enhancement} = 20 \log \left(\frac{\text{ABF peak-to-peak signal amplitude}}{\text{beamsteer peak-to-peak signal amplitude}} \right) . \qquad \text{(III-1)}$$

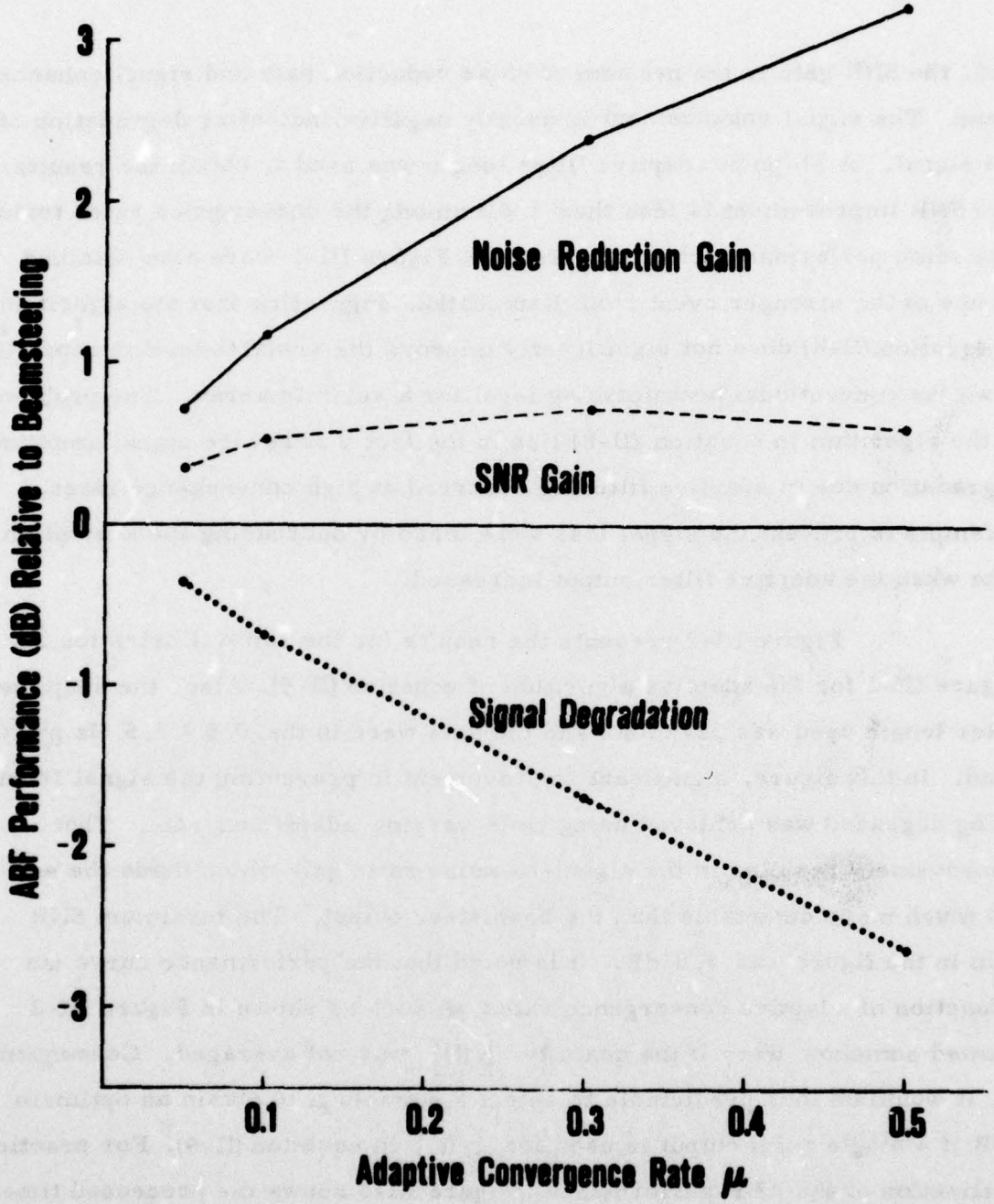


FIGURE III-1

THE ADAPTIVE BEAMFORMING (ABF) PERFORMANCE RELATIVE TO BEAMSTEERING VERSUS ADAPTIVE CONVERGENCE RATES. THE RESULTS ARE BASED ON THE ALGORITHM IN EQUATION (II-8). SIGNAL WAS FROM EASTERN KAZAKH ON JULY 23, 1976. ADAPTIVE FILTER LENGTH WAS 31-POINT, 17 CHANNELS WERE USED FOR BEAMSTEERING, AND SINGLE-CHANNEL DATA WERE BANDPASS (0.5-3.5 Hz) FILTERED

And, the SNR gain is the net sum of noise reduction gain and signal enhancement. The signal enhancement is usually negative indicating degradation of the signal. A 31-point adaptive filter length was used to obtain the results. The SNR improvement is less than 1 dB among the convergence rates tested. The same performance characteristics of Figure III-1 were also obtained by use of the stronger event from Kamchatka, suggesting that the algorithm in equation (II-8) does not significantly improve the signal detection capability from the conventional beamforming level for a seismic array. The problem of the algorithm in equation (II-8) lies in the fact that severe signal amplitude degradation due to adaptive filtering occurred at high convergence rates. Attempts to prevent the signal loss were made by decreasing the adaptation rate when the adaptive filter output increased.

Figure III-2 presents the results for the same illustration as Figure III-1 for the adaptive algorithm of equation (II-9). Also, the adaptive filter length used was 31-points and the data were in the 0.5 - 3.5 Hz passband. In this figure, significant improvement in preventing the signal from being degraded was achieved using time-varying adaptation rate. That improvement resulted in the signal-to-noise ratio gain which made the signal much more detectable than the beamsteer output. The maximum SNR gain in the figure was 4.8 dB. It is noted that the performance curve (as a function of adaptive convergence rates, μ) such as shown in Figure III-2 showed somehow wavy if the quantity $|y(t)|$ was not averaged. Consequently, it would be less predictable to select a suitable μ to obtain an optimum SNR if a single point output is used for $|y(t)|$ in equation (II-9). For practical realization of the ABF performance, Figure III-3 shows the processed time traces. The first trace is the beamsteer output beam, and the second trace is the adaptive output beam for $\mu = 5.0$ using the algorithm in equation (II-9). Both traces were plotted with the same scale factor. Therefore, noise elimination is seen in the figure on the adaptive beam as compared with the

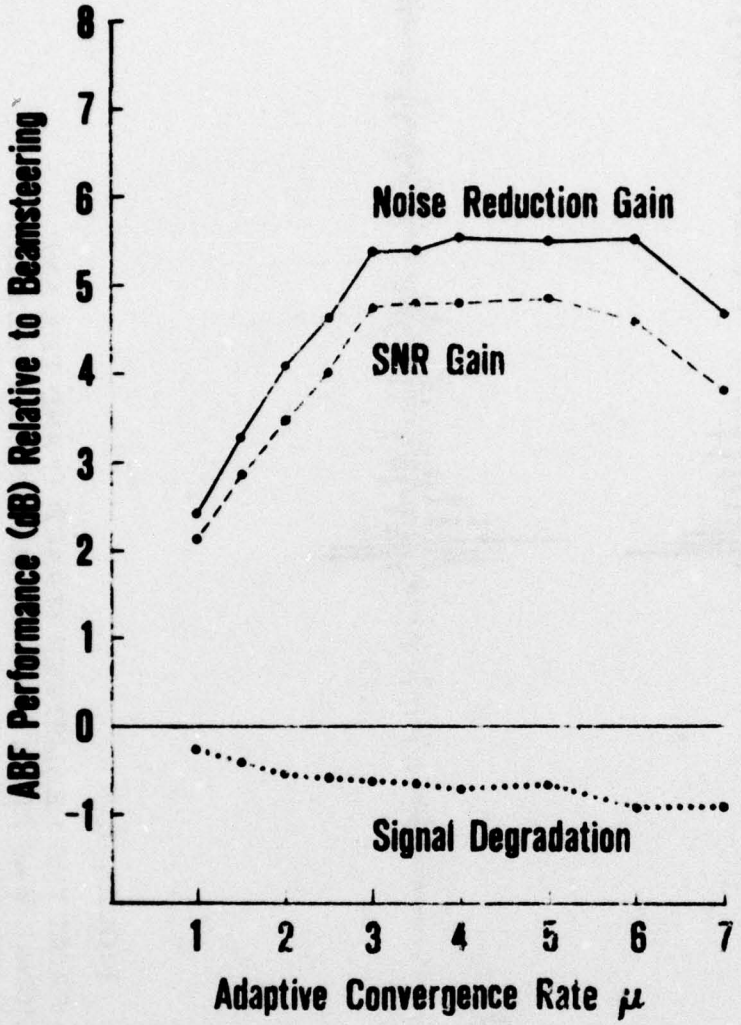


FIGURE III-2

THE ABF PERFORMANCE RELATIVE TO BEAMSTEERING VERSUS THE ADAPTIVE CONVERGENCE RATE. THE SAME SIGNAL AS IN FIGURE 1 WAS USED IN THIS FIGURE. THE RESULTS ARE BASED ON THE ADAPTIVE ALGORITHM IN EQUATION (II-9). ADAPTIVE FILTER LENGTH WAS 31-POINTS AND 17 CHANNEL DATA IN (0.5-3.5 Hz) PASSBAND WERE USED FOR BEAMFORMING

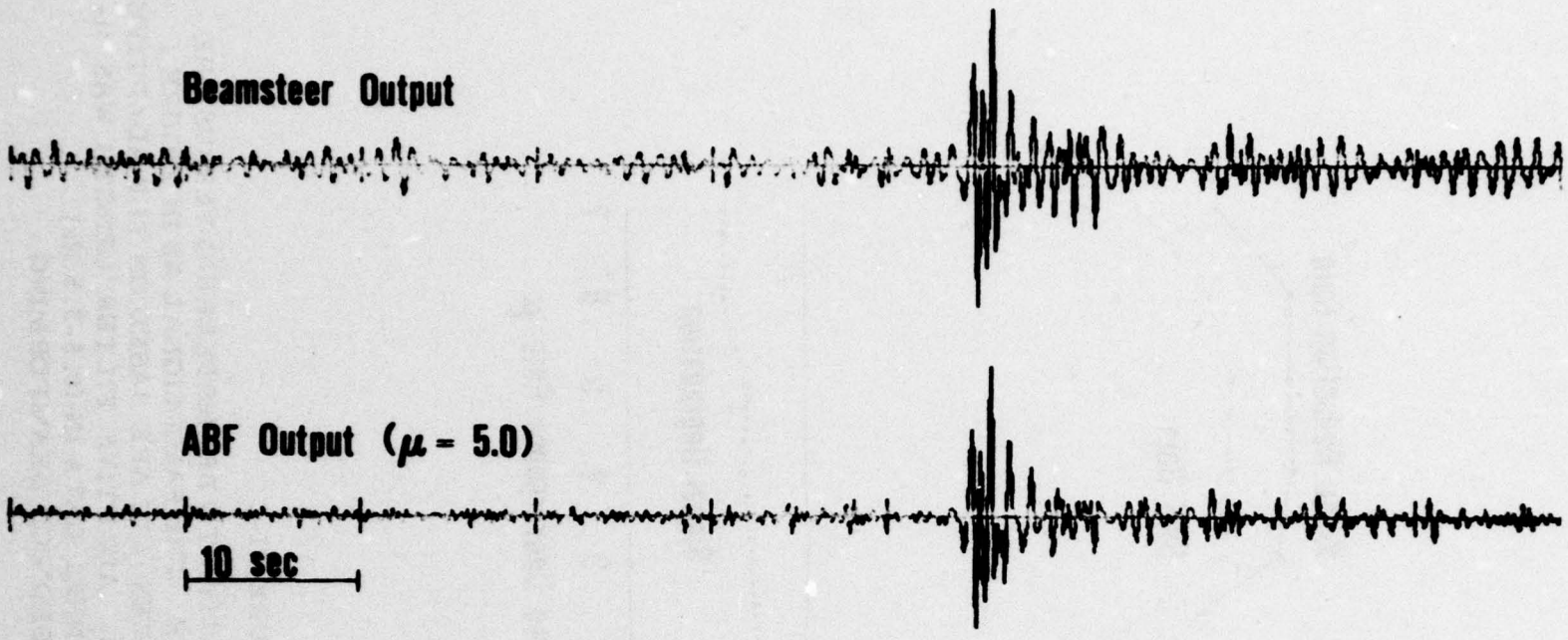


FIGURE III-3

PROCESSED TRACES OBTAINED FROM THE BEAMSTEER (TRACE 1) AND THE ABF (TRACE 2) PROCESSORS. THE SIGNAL WAS FROM EASTERN KAZAKH ON JULY 23, 1976. ADAPTIVE FILTER LENGTH WAS 31-POINT AND 17 CHANNEL DATA IN (0.5-3.5 Hz) PASSBAND WERE USED FOR BEAMFORMING

beamsteer output. Considering the fact that 17-channel data were used for forming the beam traces, adaptive beamforming performance in Figure III-3 would be approximately equivalent to that of a 51-channel array using conventional beamforming processor if $\sqrt{M}$ improvement, where M is the number of channels of an array, is assumed for array noise reduction and if the signal degradation is neglected.

2. Low Passband

In the lower frequency passband (0.5 - 1.1 Hz), the adaptive filter was found to have much more noise reduction capability and also more severe signal amplitude degradation than in the 0.5 - 3.5 Hz passband. A noise study using high resolution frequency-wavenumber spectral analysis for the KSRS short-period array indicated that noise at the KSRS is mostly surface-wave mode energy with a propagating velocity less than 4.0 km/second in the lower frequency passband (<1.0 Hz) and is compressional mode energy with a propagating velocity greater than 6 km/second in the higher frequency passband (Prahl et al., 1975). Also, since noise is much more correlated in the lower frequency passband than in the higher frequency passband, one would expect that the adaptive filter would eliminate noise more in the low passband than in the higher passband. With the same signal from eastern Kazakh, Figure III-4 presents the adaptive filter performance relative to beamsteering versus the adaptive convergence rates in the low passband, where a 31-point adaptive filter length and 17 channels of data were used. The optimum adaptive performance seems to be at $\mu = 2.0$, where the relative noise gain was 19.5 dB, signal loss was -2.7 dB, and the resultant relative SNR gain was 16.8 dB over the beamsteer processor.

Figure III-5 presents the time traces of array beam outputs for the beamsteer processor and the adaptive beamforming processor at

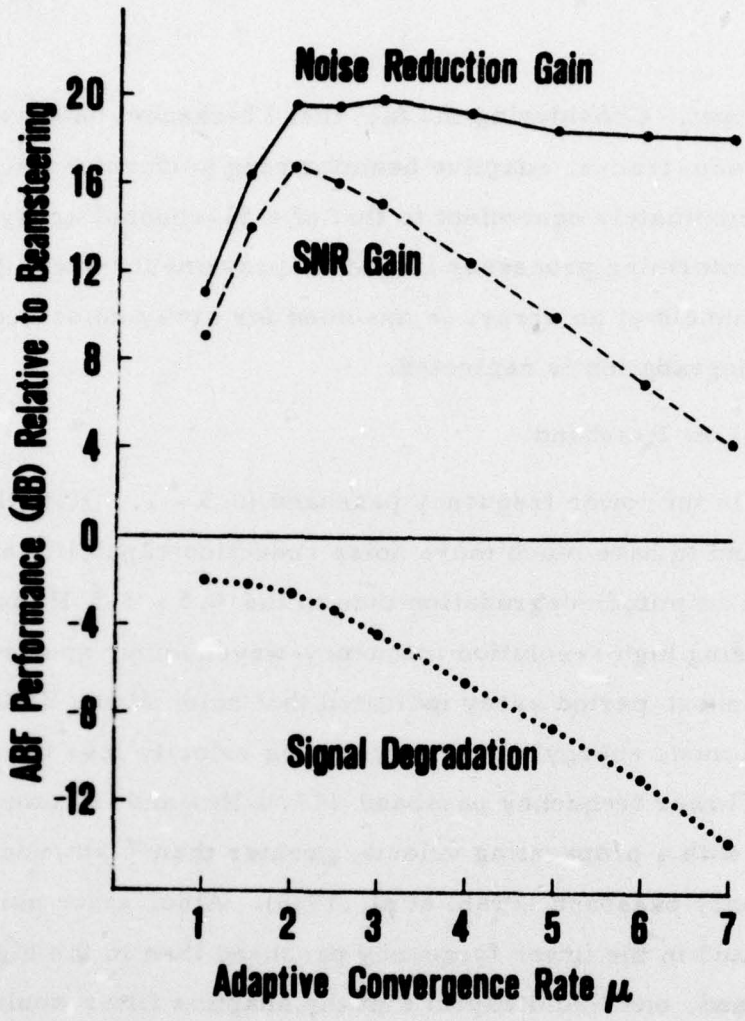


FIGURE III-4

THE ABF PERFORMANCE RELATIVE TO BEAMSTEERING VERSUS THE ADAPTIVE CONVERGENCE RATE. THE RESULTS ARE BASED ON THE ALGORITHM IN EQUATION (II-9). ADAPTIVE FILTER LENGTH WAS 31-POINTS AND 17 CHANNELS WERE USED. THE DATA WERE IN 0.5-1.1 Hz PASSBAND

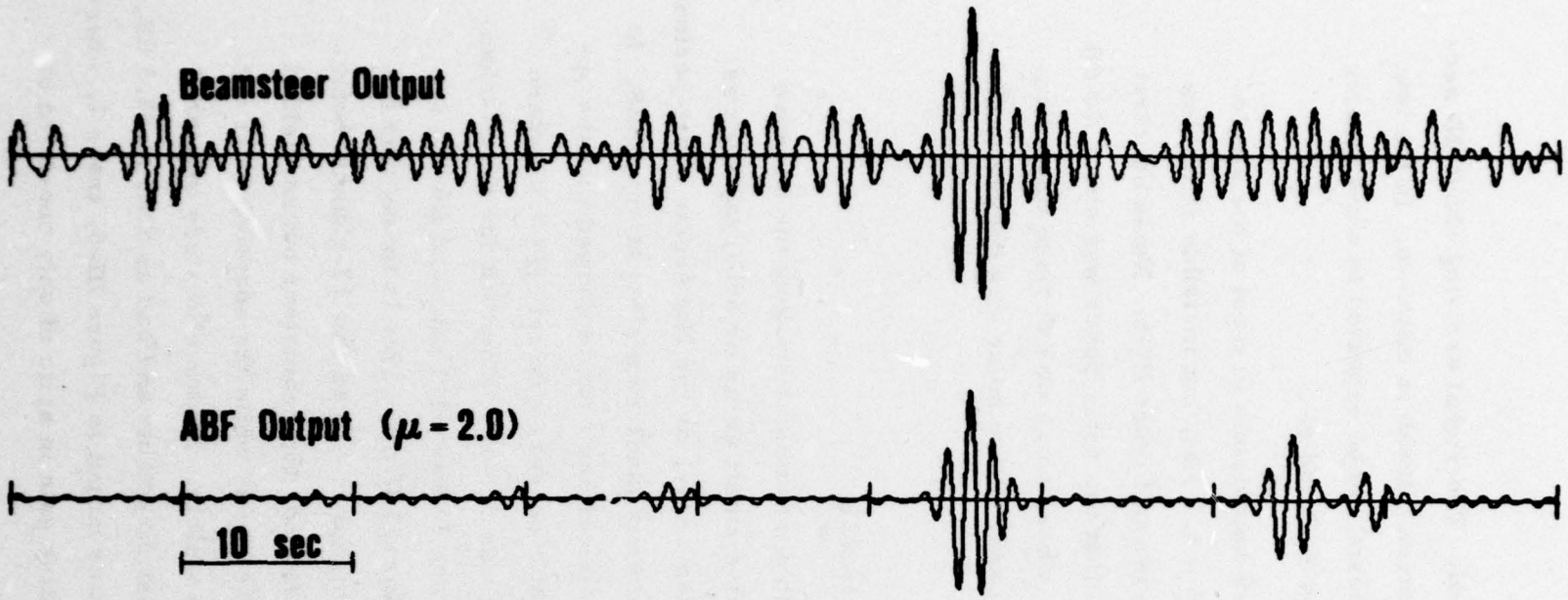


FIGURE III-5

PROCESSED TRACES OF EASTERN KAZAKH EVENT OBTAINED FROM THE BEAMSTEER (TRACE 1) AND THE ABF (TRACE 2) PROCESSORS. THE DATA WERE BANDPASS (0.5-1.1 Hz) FILTERED AND 17 CHANNEL BEAMFORMED. A 31-POINT ADAPTIVE FILTER LENGTH WAS USED.

μ = 2.0 for the low frequency passband. The signal arriving about 20 seconds after the P-wave signal from eastern Kazakh is unknown. In the low frequency passband, the ABF output beam can be expected to show clearly the secondary P-wave phases, such as PcP and pP.

The signal in Figure III-5 was visible in most of the single-channel data in the wide passband (0.5 - 3.5 Hz), but invisible in the low frequency passband whose data are shown in Figure III-6. Noise spectral analysis (Prahl et al., 1975) indicated that the noise power was about 20 dB higher in the low frequency passband, where noise was surface wave dominant, than in the high frequency passband, where noise was bodywave dominant.

C. INNER-RING ARRAY PERFORMANCE

An interesting question to answer is: How does the adaptive beamforming filter perform in a relative small array or subarray such as the KSRS long-period array, the Iranian array, or the Norwegian short-period subarray? To answer this, we used the six inner ring sites at the KSRS. In the wide passband, the six channel beamforming outputs showed that the optimum performance for the ABF was at a convergence rate μ = 7.0, where the SNR gain relative to beamsteering was 5.5 dB. The SNR for the 17-channel beamsteer output (Figure III-3, trace 1) was 31.1 dB, and for the six channel inner ring beamsteer output was 27.7 dB. This is to say that the six channel adaptive output had 2 dB higher SNR than the 17-channel beamsteer output. In the low frequency passband, the beamsteer output yielded signal estimates apparently at the noise level, while the adaptive filter output clearly showed that the signal was visible. Systematic study indicated that at μ = 6.0, the signal was the most detectable and had an SNR of 28.3 dB. Compared with the 17-channel beamsteer output in Figure III-5, trace 1, where the SNR was 22.3, it had a 6 dB relative gain in spite of only one-third of

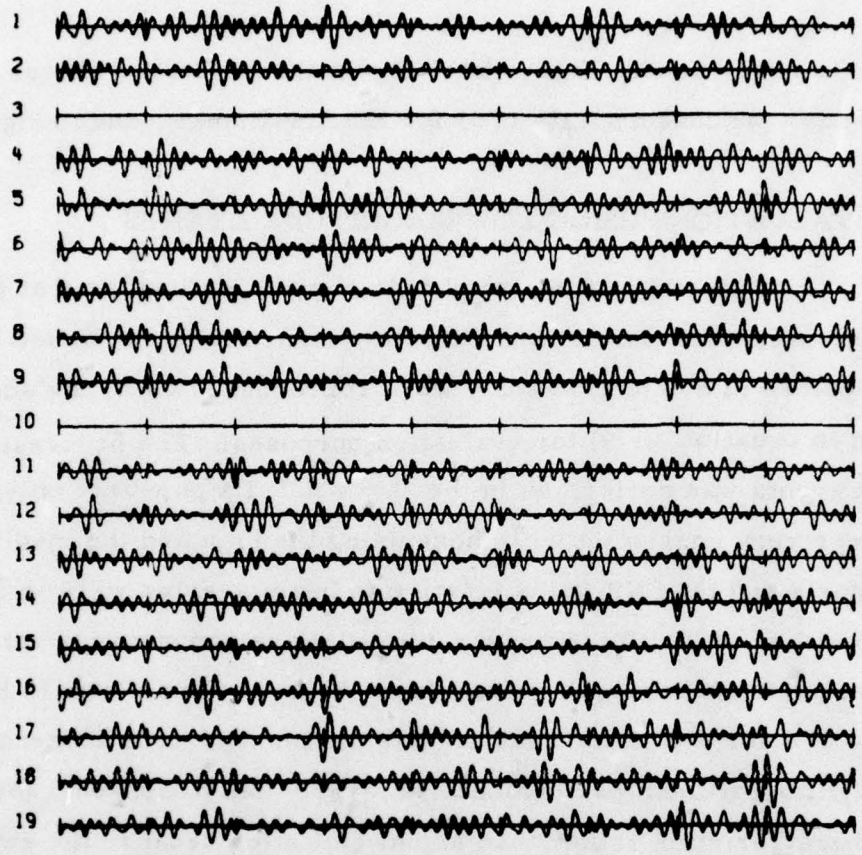


FIGURE III-6

SINGLE-CHANNEL DATA FOR THE EASTERN KAZAKH EVENT IN THE 0.5-1.1 Hz PASSBAND

the size of array used. Figure III-7 shows the processed traces of beamsteer and adaptive processors (μ = 6.0) for the six-channel inner ring array.

D. EVALUATIONS USING LOW MAGNITUDE EVENTS

A number of low amplitude signals (defined as that the expected signals were not visible in the single-channel data) which had been processed before in a detection study were reprocessed using the adaptive algorithm in equation (II-9) for evaluation purposes. The processing for the set of weak events was performed in the 0.5 - 3.5 Hz passband only. The results were very consistent with those using the high and the medium amplitude signals and the SNR gains relative to beamsteering were in general in the range 4.6 - 6.7 dB. However, the adaptive convergence rates, μ, for optimum performance were shifted from 3.0 - 6.0 as shown in Figure III-2 to 0.5 - 1.0 for the set of weak signals processed. It is contended that the shift of μ for optimum performance is largely due to seasonal (or directional) noise characteristics rather than signal statistics because the set of weak signals was recorded in November of 1974, while the eastern Kazakh event was in July of 1976. This contention has been confirmed by a signal-plus-scaled-noise study in Subsection III-F where it shows that μ (for optimum performance) increases as noise levels are scaled up. As an example, Figure III-8 presents the processed traces for an event from Tibet. The first trace is the beamsteer output, and the second and the third are the adaptive beamforming outputs with μ = 0.75 and 1.5, respectively. The signal amplitudes on the beamsteer output are just at the noise levels and not visible in this case. But the adaptive beamformer extracted the signal by eliminating noise so that the signal is clearly visible. When higher convergence rate is used, the signal amplitudes of the initial arrival were degraded as shown in the last trace in Figure III-8. The low magnitude processing results are presented in Appendix A.

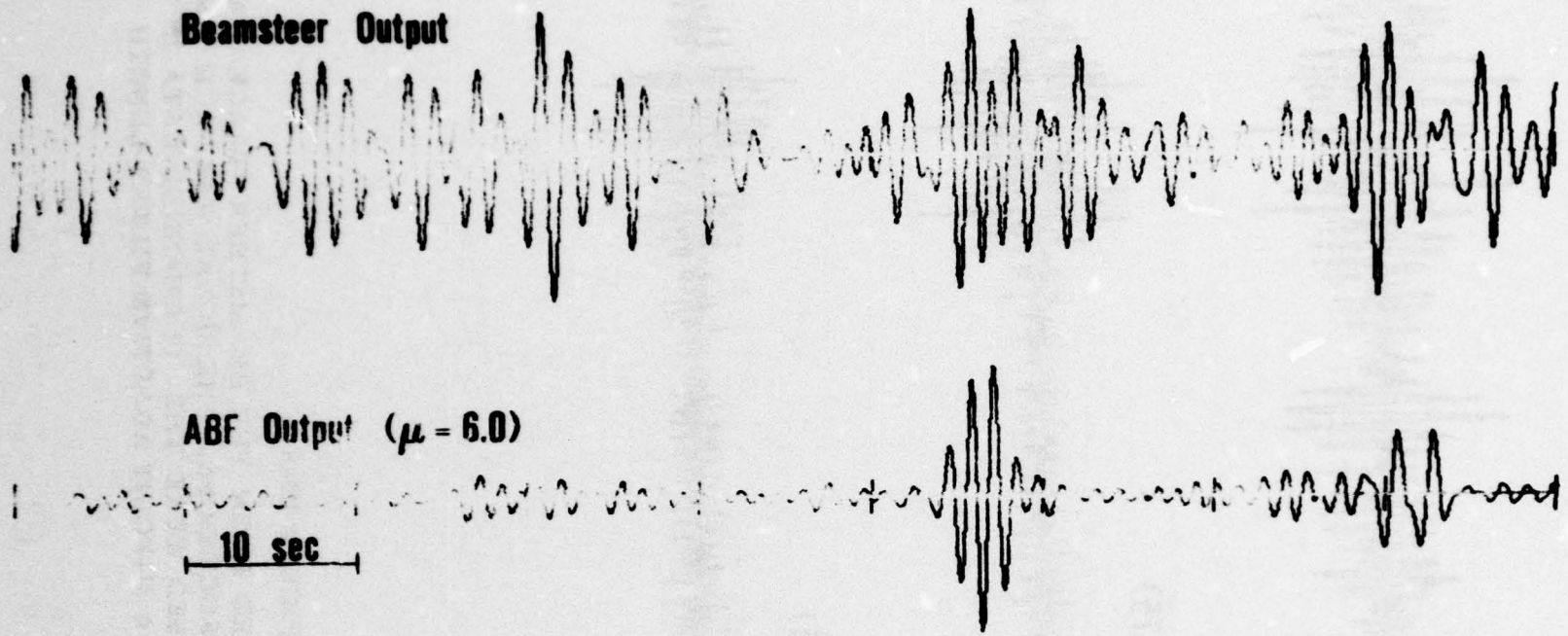


FIGURE III-7

PROCESSED TRACES OF EASTERN KAZAKH EVENT OBTAINED FROM THE BEAMSTEER (TRACE 1) AND THE ABF (TRACE 2) PROCESSORS. ONLY SIX INNER-RING CHANNELS WERE USED FOR BEAMFORMING. THE DATA WERE IN 0.5-1.1 Hz PASSBAND AND A 31-POINT ADAPTIVE LENGTH WAS USED FOR THE ABF

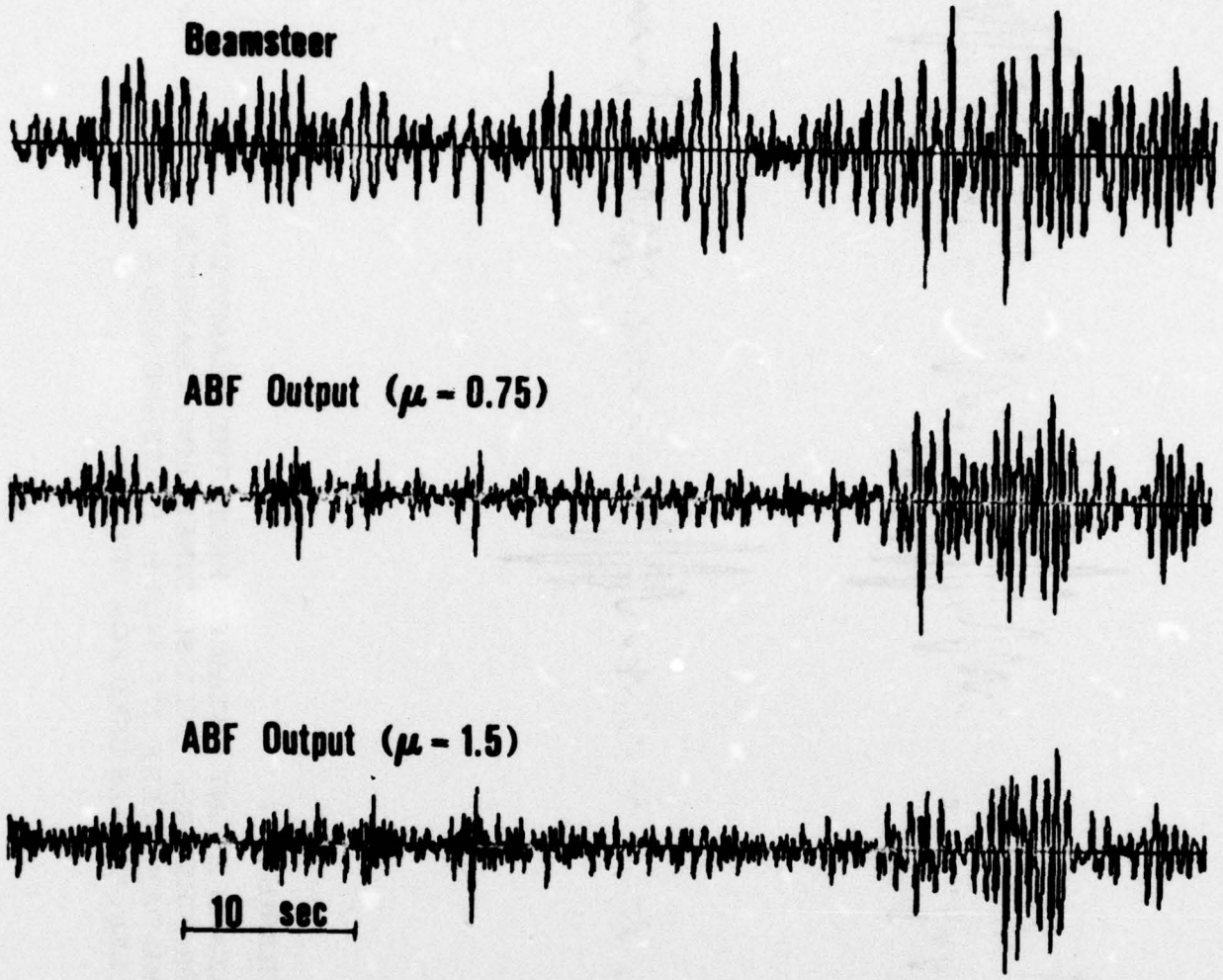


FIGURE III-8

PROCESSED TRACES OBTAINED FROM THE BEAMSTEER (TRACE 1) AND THE ABF (TRACES 2 AND 3) PROCESSORS. THE SIGNAL WAS FROM TIBET ON NOVEMBER 10, 1974. USED WERE THE 19 CHANNEL DATA IN THE 0.5-3.5 Hz PASSBAND AND A 31-POINT ADAPTIVE FILTER LENGTH

E. RESPONSE PATTERN

Using the same signal from the presumed explosion in eastern Kazakh, the response pattern was measured for the beamsteer and ABF processors. Figure III-9 shows the peak-to-peak amplitude response versus the azimuths of the KSRS short-period array. The results indicated that the beamsteer and the ABF responses follow about the same pattern with 60° beamwidth at -6 dB. A lack of symmetry from the steering azimuth (304°) was possibly due to the fact that two channels were deleted from the input because of bad data as shown in Figure III-6. Figure III-10 presents the signal-to-noise ratio versus the azimuths. The SNRs were computed the same way described earlier in Subsection III-A (but with slightly larger noise gate). The ABF maintains its processing gains over beamsteering within the mainlobe and performs much better beyond the mainlobe.

Figure III-11 shows the peak-to-peak amplitude response versus the epicentral delta which indicates the variations of apparent P-wave velocity used in computing the time-delay parameter for array beamforming. Peak-to-peak amplitude at $\Delta = 36.1^{\circ}$ was used as a reference point for response computation. The figure suggests that the maximum amplitude is at 46.1° of epicentral delta, corresponding to 14.47 km/s of velocity, instead of 36.1° which is the epicentral delta for the source, corresponding to 13.17 km/s. The slight shift of apparent wave velocity to obtain the maximum power steering appeared as no surprise. The ray-path of the P-wave was possibly from a higher velocity zone to the lower velocity zone near the receiving array and in this situation the ray was bent more upward in the crust than the normal incident angle. That would appear as a higher apparent velocity to the array. Figure III-11 indicates that, for teleseismic events, the epicentral delta is not a critical parameter for both the beamsteer and ABF processors. Figure III-12 presents the computation of signal-to-noise ratio versus the epicentral delta. The ABF maintains the same performance relative to beamsteering as shown in the figure.

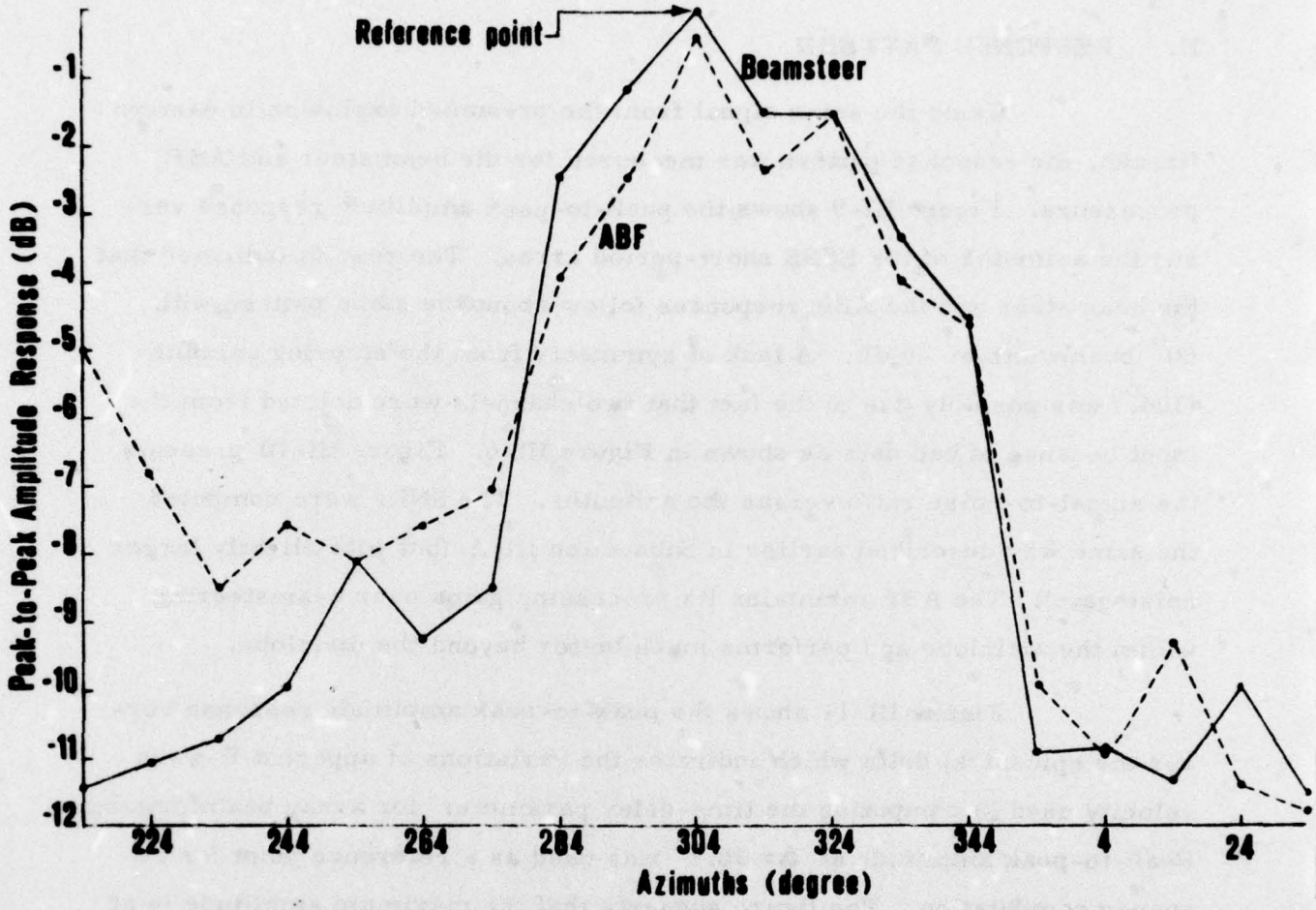


FIGURE III-9

MEASURED DIRECTIVITY (AZIMUTH) RESPONSE PATTERN
FOR THE EVENT FROM EASTERN KAZAKH

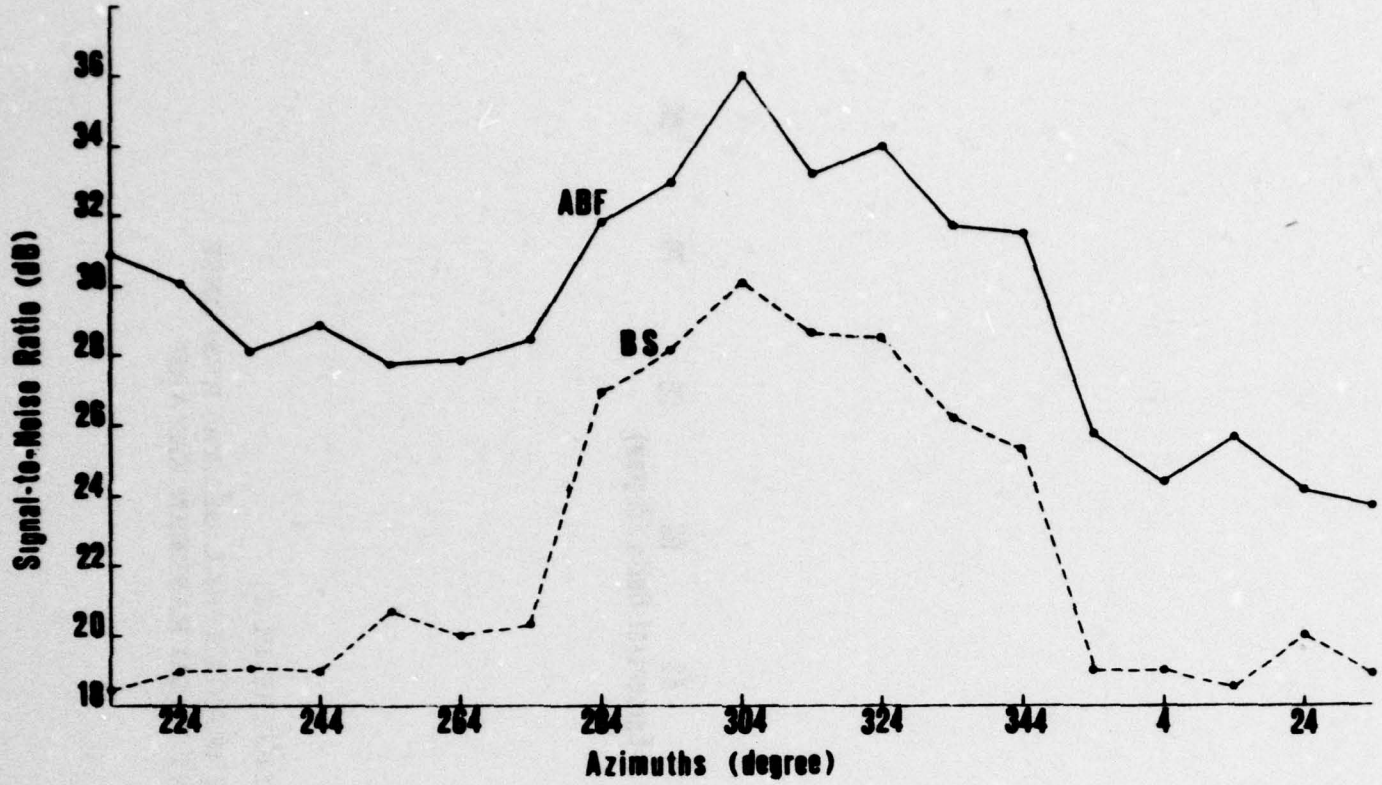


FIGURE III-10

MEASURED SNR VERSUS AZIMUTH

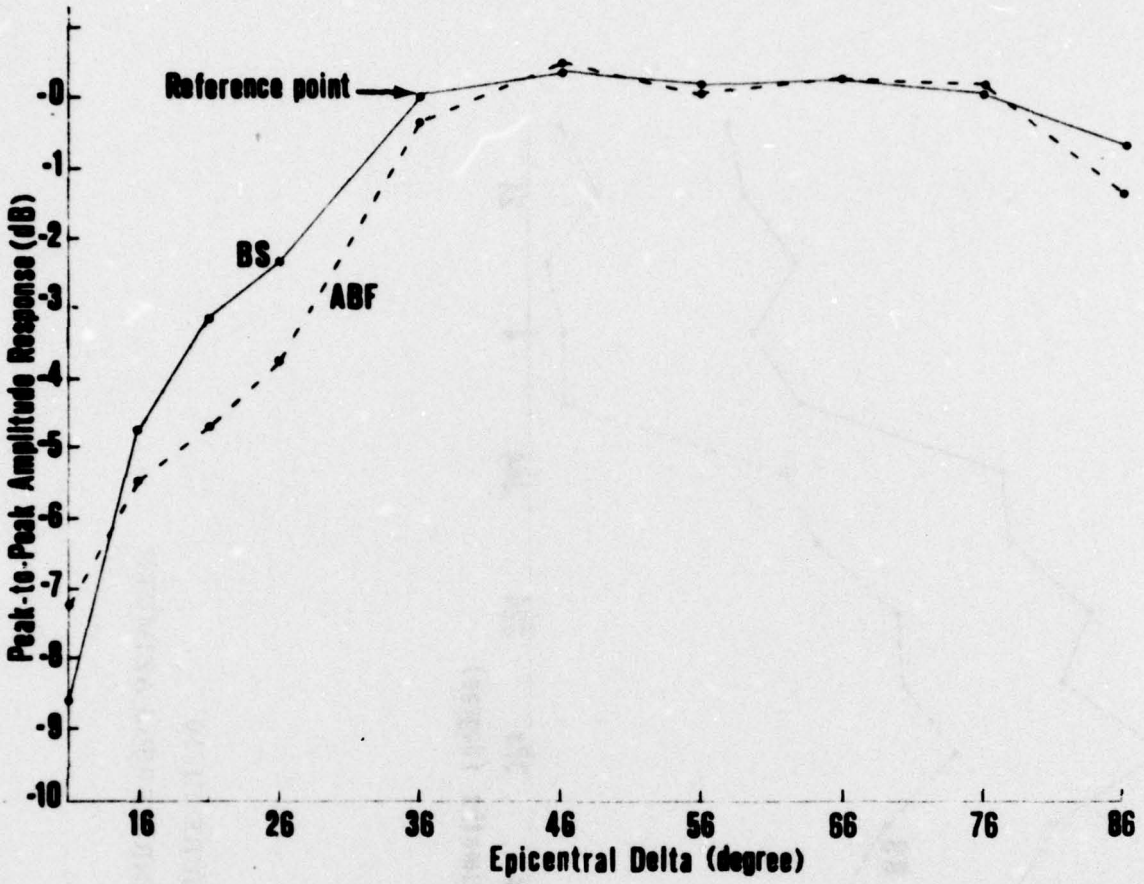


FIGURE III-11

MEASURED VELOCITY (EPICENTRAL DELTA) RESPONSE
FOR THE EVENT FROM EASTERN KAZAKH

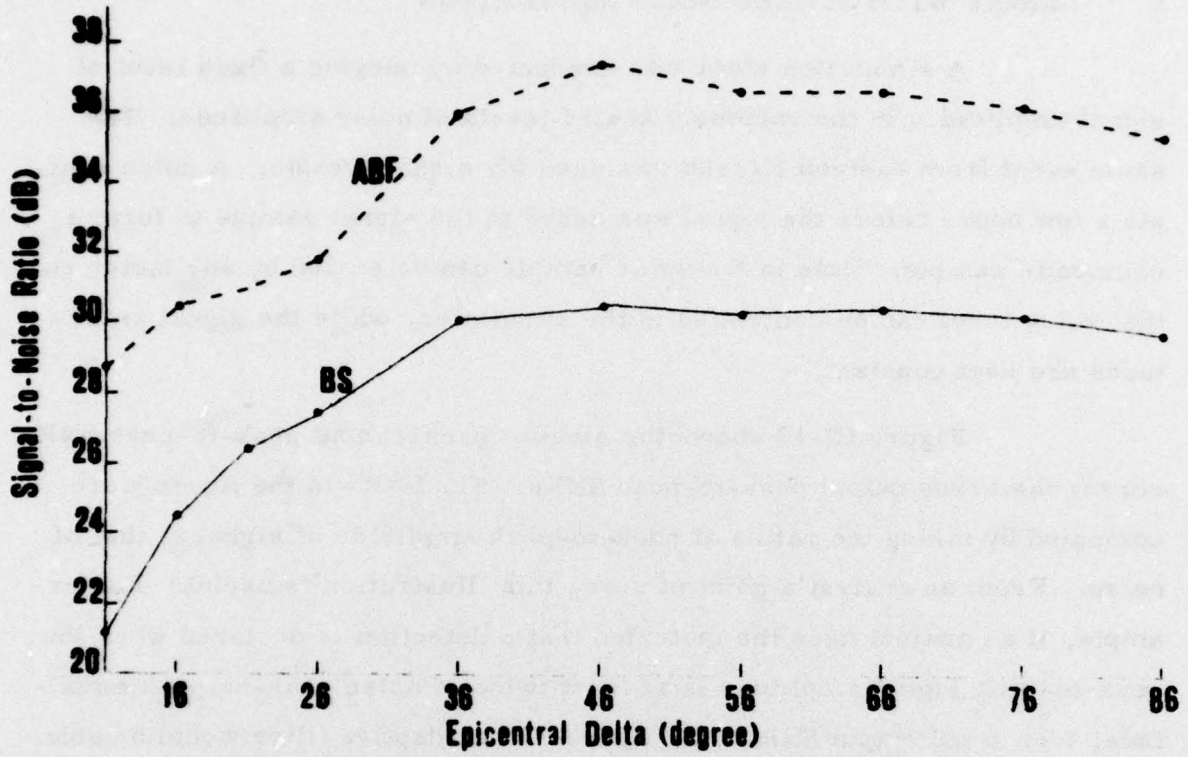


FIGURE III-12

MEASURED SNR VERSUS EPICENTRAL DELTA
(EVENT AZIMUTH = 304.3° AND EVENT DELTA = 36.1°)

F. SIGNAL WITH SCALED NOISE SIMULATION

A simulation study was conducted by burying a fixed level of signal amplitudes in the variously scaled levels of noise amplitude. The same event from eastern Kazakh was used for signal sample. A noise sample a few hours before the signal was added to the signal sample to form a composite sample. Data in the noise sample can be scaled by any factor so that noise level can be controlled in the simulation, while the signal amplitudes are kept constant.

Figure III-13 shows the single-channel input peak-to-peak SNRs versus the array output peak-to-peak SNRs. The SNRs in the figure were computed by taking the ratios of peak-to-peak amplitude of signal to that of noise. From an analyst's point of view, this illustration is useful. For example, if an analyst uses the criterion that a detection is declared when the peak-to-peak signal amplitude is at least twice of noise peak-to-peak amplitude, i.e. 6 dB output SNR in the figure. The adaptive filter would be able to achieve a threshold reduction of about 6 dB (0.3 m_b unit). That is, the analyst can correctly claim more detection of low amplitude signal (or low magnitude events) by the ABF processor than by the beamsteer processor if he operates the two processor at the same output SNR. Looking from the other angle in the figure, for a given input single-channel SNR level, the differences of array outputs between the beamsteer and ABF processors are the processing gains which can be interpreted as the false alarm reduction if the analyst uses higher output SNR for the ABF than for the beamsteer processor to achieve the same detection rate. Hence the figure can be interpreted as the "operating characteristic" to compare the performance between the two processors.

Figure III-14 shows the same illustration as in Figure III-13, but the SNRs were computed by taking the ratio of peak-to-peak signal amplitude to RMS noise amplitude. The interpretation for threshold reduction

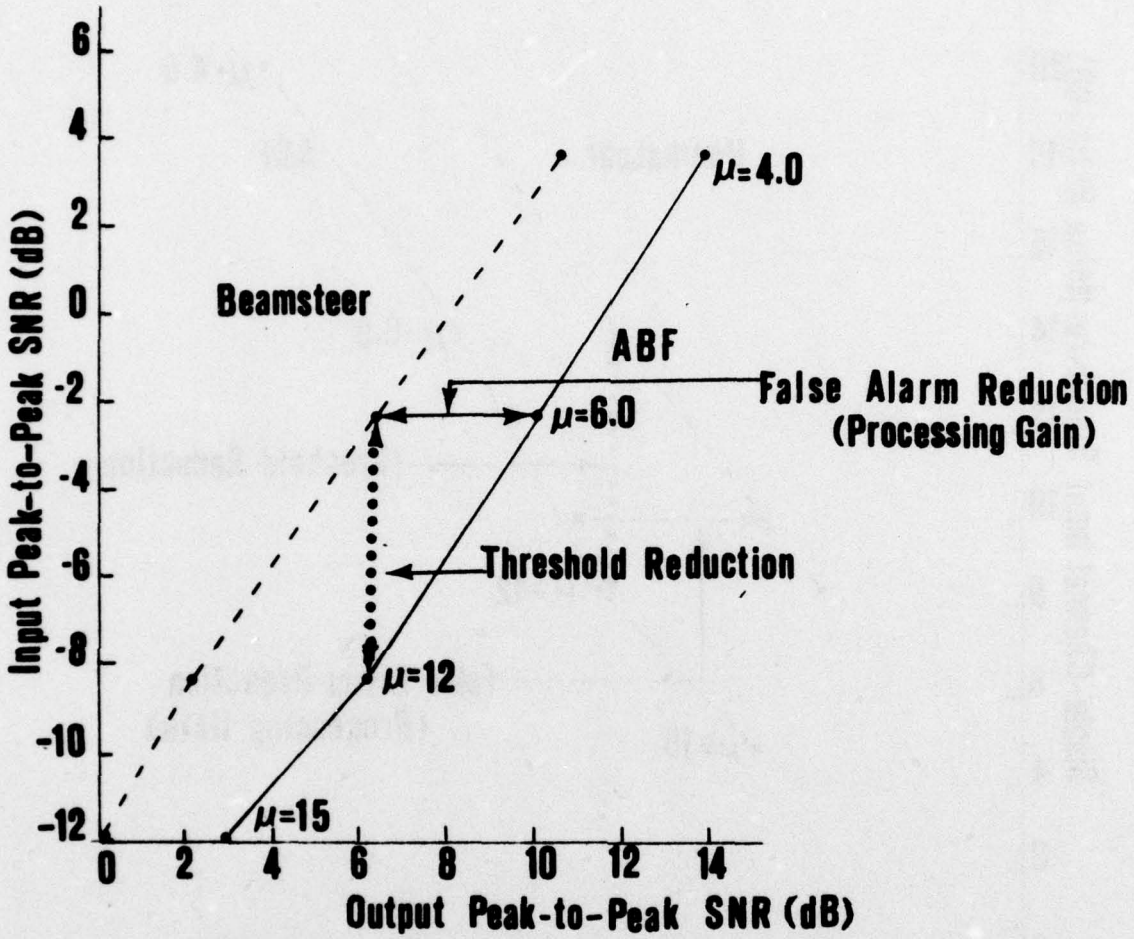


FIGURE III-13

AMPLITUDE-WISE OPERATING CHARACTERISTICS

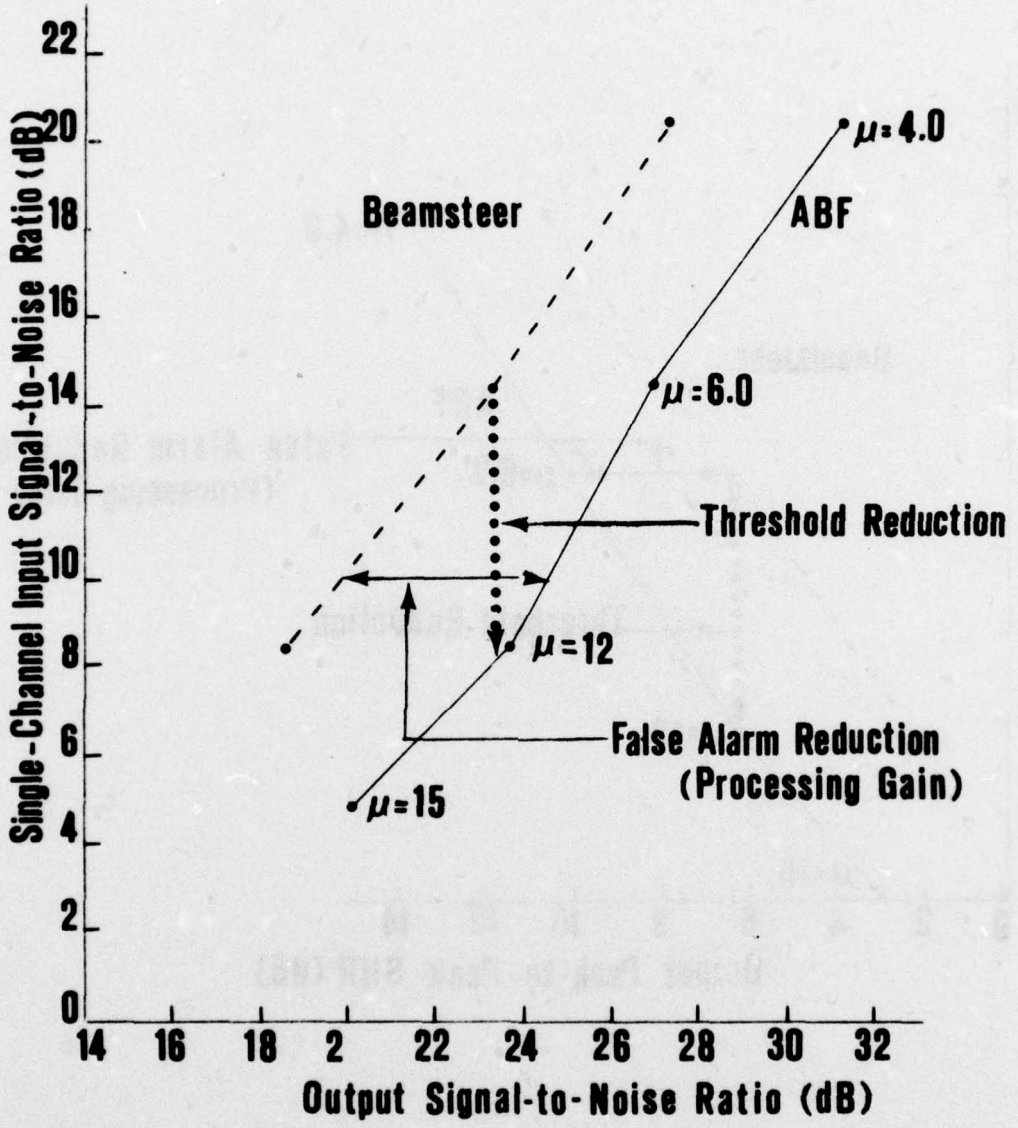


FIGURE III-14

RMS NOISE AND SIGNAL AMPLITUDE-WISE
OPERATING CHARACTERISTICS

as well as for false alarm reduction (processing gain) is shown in the figure. The processing gains (with natural noise and signal) in general are in the range of 4.5 - 6.5 dB as discussed in Subsection III-D.

G. ADAPTIVE FILTER LENGTH

To study the ABF performance as a function of the filter length, Figure III-15 shows the ABF SNR gains relative to beamsteering versus the convergence rate μ. Processing with a number of filter lengths was conducted: namely, 7, 15, 31, 41, 51, 61 points. With 31, 41, 51, and 61 point filters, not much differences in performance are obtained. Hence, only four curves for 7, 15, 31, 41 point filters, respectively, are shown in the figure. We concluded that the 31 point filter is practically optimum for the ABF in the wide passband (0.5 - 3.5 Hz) of short-period data.

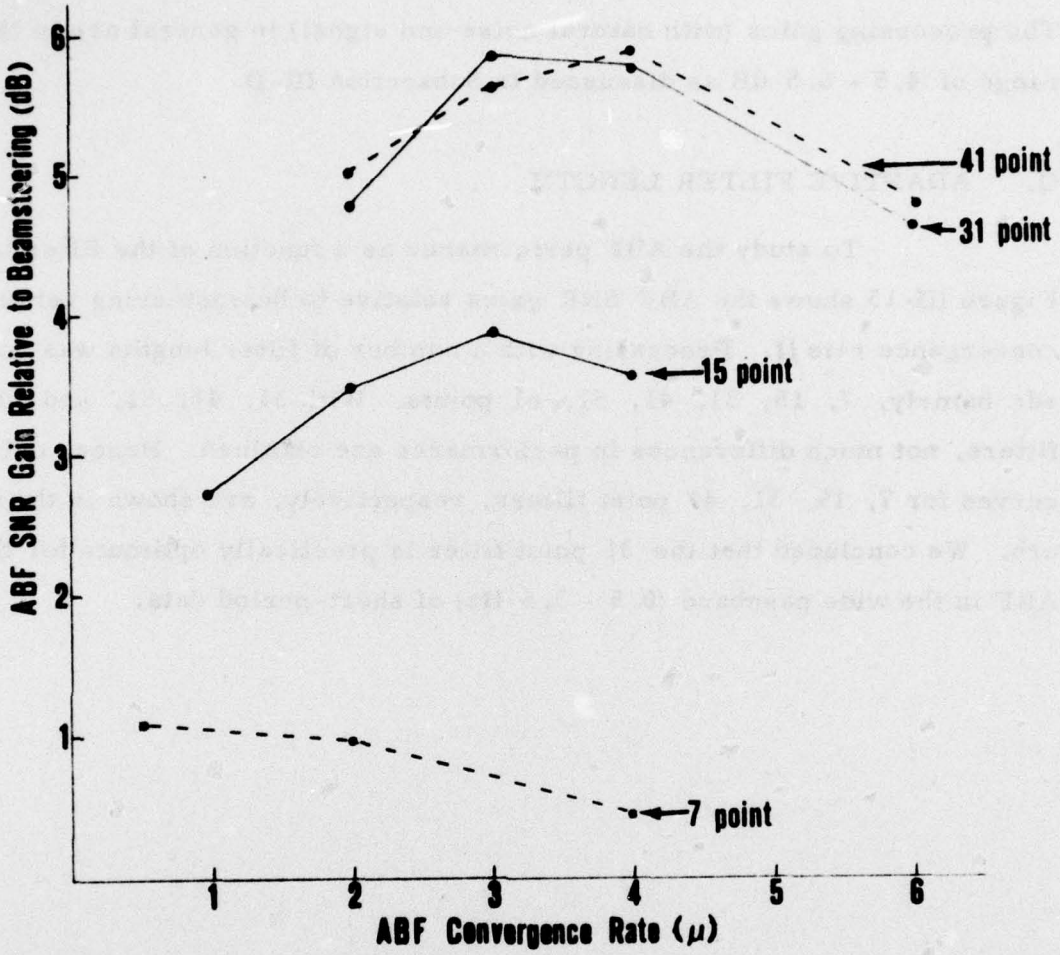


FIGURE III-15

ABF PERFORMANCE FOR VARIOUS
ADAPTIVE FILTER LENGTHS

SECTION IV

CONCLUSION AND FURTHER WORK FOR IMPLEMENTATION

A. CONCLUSION

The present time-varying adaptation rate, constrained minimum power adaptive beamforming algorithm and its performance have been described. The algorithm requires no a-priori knowledge of noise or signal. The filter weights were corrected for every 200 iterations in order to correct the round-off errors during the processing. Iterations with the adaptive algorithm are stable, and it is feasible that the ABF processor can be practically implemented as a real-time front-end seismic processor.

The algorithm achieved signal-to-noise ratio gain relative to beamsteering at about 17 dB in the low passband (0.5 - 1.1 Hz) of short-period seismic data. The ABF performance in this passband can be utilized to separate and measure secondary phases. Detection and measurement of the low frequency band P-waves may also provide important information for discriminating explosions from earthquakes. The apparent mechanism for attaining the gain in this band was the elimination of coherent Rayleigh wave noise.

In the wide passband (0.5 - 3.5 Hz) of short-period seismic data, the adaptive filter in general achieved about 4.5 - 6.5 dB signal-to-noise ratio improvement over the conventional array beamforming method using the high, medium, and a number of low amplitude signals. As far as detection capability is concerned, the gain of the adaptive filter is equivalent in effect to tripling or quadrupling the array size on the basis of conventional beamsteering performance. For example, adaptive beamforming of a

19-channel KSRS short-period array yields a performance equivalent to that of a 57- or 76-channel array processed by the conventional beamforming method.

Study of directivity (azimuth) response indicated that the beamsteer and ABF response pattern are very close to each other in the 60^{o} beamwidth. This result suggested that the present ABF would not be degraded by limited number of beams formed in a detection system. As a matter of fact, the ABF maintained its relative performance in the mainlobe and performed better than the beamsteer processor beyond the mainlobe as shown in Figure III-10.

Simulation by signal added to various levels of noise amplitude suggested that the processing gain and threshold reduction are consistent and are typically in the range of 4 - 6 dB. The ABF processing gain can be interpreted as false alarm reduction, while the ABF threshold reduction as increased detection capability (Figures III-13, III-14).

B. FURTHER WORK FOR IMPLEMENTATION

Further research on the present adaptive beamforming processor for practical implementation may be needed. Work on operational parametrization and automatic control is suggested here.

As noted before, the actual adaptation rate $\lambda(t)$ in equation (II-5) for this adaptive algorithm is highly time-varying and is inversely proportioned to the absolute value of filter output amplitude and the total filter input power. In the situations that the number of input channels is varied significantly, the total input power P(t) changes considerably. Hence μ would be dependent on P(t). To obtain a more universal and perpetual operational input parameter μ, one can use the averaged input power, instead of the total input power. However, our results suggested that $|y(t)|$ in equation (II-9) was more sensitive than P(t) as far as choosing a proper μ

is concerned. Various tests on different data indicated that the optimum μ is roughly proportional to the RMS noise amplitude of the filter output with $\mu' = \mu/\sigma \cong 1.6$, where σ is the RMS noise amplitude of filter output. Therefore, one can divide $|y(t)|$ in equation (II-9) by its exponentially smoothed long-term average to make μ less data dependent and physically dimensionless.

During the research work, channel selection or data quality control was done manually by manpower. For implementing the adaptive beamformer in a real-time front-end (or post front-end) detection system, automatic quality control is needed, and the existing techniques (Shen, 1976b) can be applied for this purpose.

On the basis of low passband processing, we anticipated that the adaptive beamforming processor would perform much better with long-period seismic array data. This adaptive beamformer may also have successful performance in other fields, such as acoustics and electromagnetics.

SECTION V
REFERENCES

Barnard, T. E., and L. J. O'Brien, 1974, An Evaluation of Adaptive-Beamforming Techniques Applied to Recorded Seismic Data; Technical Report No. 8, VELA Network Evaluation and Automatic Processing Research, Texas Instruments Incorporated, Equipment Group, Dallas, Texas.

Booker, A., and C. Y. Ong, 1971, Multiple-Constraint Adaptive Filtering; Geophysics, v. 36, p. 498-509.

Burg, J. P., Booker, A. H. and Holyer; 1967, Adaptive Filtering of Seismic Array Data, Advanced Array Research, Report No. 1, Texas Instruments Incorporated, Science Service Division, Dallas, Texas 75222, and also a number of subsequent technical reports by Booker and his co-workers.

Capon, J., R. J. Greenfield, and R. J. Kolker, 1967, Multidimensional Maximum-Likelihood Processing of a Large Aperture Seismic Array; Proceedings of the IEEE, v. 55, no. 2, p. 192-211.

Claerbout, J. F., 1976, Fundamentals of Geophysical Data Processing; McGraw-Hill, New York, NY.

Frost, O. L. III, 1972, An Algorithm for Linearly Constrained Adaptive Array Processing; Proceedings of the IEEE, v. 60, no. 8, p. 926-935.

Gangi, A. F., and B. S. Byun, 1975, The Corrective Gradient Projection Method and Related Algorithms Applied to Seismic Array Processing; Geophysics, v. 41, no. 5, p. 970-984.

Griffiths, L. J., 1969, A Simple Adaptive Algorithm for Real-Time Processing in Antenna Arrays; Proceedings of IEEE, v. 57, p. 1696-1704.

Griffiths, L. J., F. R. Smolka, and L. D. Trembly, 1977, Adaptive Deconvolution: A new technique for processing time-varying seismic data; Geophysics, v. 42, p. 742-759.

Levin, M. J., 1964, Maximum-Likelihood Array Processing; Lincoln Laboratory Report, 31 December 1964.

Lintz, P. R., 1968, Principles of Wiener Auto-Adaptive Filtering; Seismic Data Laboratory Report No. 224, Teledyne, Geotech, 314 Montgomery Street, Alexandria, VA.

Prahl, S. R., W. W. Shen, and R. L. Whitelaw, 1975, Preliminary Evaluation of the Korean Seismic Research Station Short -Period Array, Technical Report No. 5, VELA Network Evaluation and Automatic Processing Research, Texas Instruments Incorporated, Equipment Group, Dallas, Texas.

Shen, W. W., 1975, A Study of Adaptive Beamforming Detection Performance on ALPA Interfering Events; Technical Report No. 6, VELA Network Evaluation and Automatic Processing Research, Texas Instruments Incorporated, Equipment Group, Dallas, Texas.

Shen, W. W., 1976, A Study of the Adaptive Beamforming Detector Using the Korean Seismic Research Station Short-Period Array; Technical Report No. 5, VELA Network Evaluation and Automatic Processing Research, Texas Instruments Incorporated, Equipment Group, Dallas, Texas.

Shen, W. W., 1976b, Evaluation of Two Automatic Signal Detectors Using the Korean Seismic Research Station Short-Period Array, Technical Report No. 3, VELA Network Evaluation and Automatic Processing Research, Texas Instruments Incorporated, Equipment Group, Dallas, Texas.

Wang, R. J., and S. Treitel, 1971, Adaptive Signal Processing through Stochastic Approximation: Geophys. Prosp., v. 19, p. 718-727.

Widrow, B., 1966, Adaptive Filters I: Fundamentals; Technical Report No. 6764-6, Systems Theory Laboratory, Stanford Electronics Laboratories, Stanford University, Stanford, California.

Widrow, B., P.E. Mantey, L.J. Griffiths, and B. B. Goode, 1967, Adaptive Antenna Systems; Proceedings of IEEE, v. 55, no. 12, p. 2143-2159.

Wiggins, R. A., and E. A. Robinson, 1965, Recursive Solution to the Multichannel Filtering Problem; JGR, v. 70, p. 1885-1892.

Winkler, L.P., and M. Schwartz, 1972, Adaptive Nonlinear Optimization of the Signal-to-Noise Ratio of an Array Subject to Constraint; J. Acoust. Soc. Am., v. 52, p. 39-51.

APPENDIX A

This appendix presents the processed time traces of weak events (defined as signals not visible in single-channel data) recorded at the KSRS short-period array in November 1974.

Thirteen events were processed, including the one presented in Figure III-8. Among those events, six of them, Figures A-1 to A-6, are visible on both the beamsteer and ABF outputs, five of them, Figures A-7 to A-10, and Figure III-8, are not visible on the beamsteer output, but are visible on the ABF, and two of them Figures A-11 and A-12 are not visible on both the beamsteer and ABF beams. In the figures the predicted arrivals on the basis of computation from the U. S. G. S. PDE bulletin are indicated by the symbol $\downarrow$, and the picked arrivals from processing by the symbol $\uparrow$.

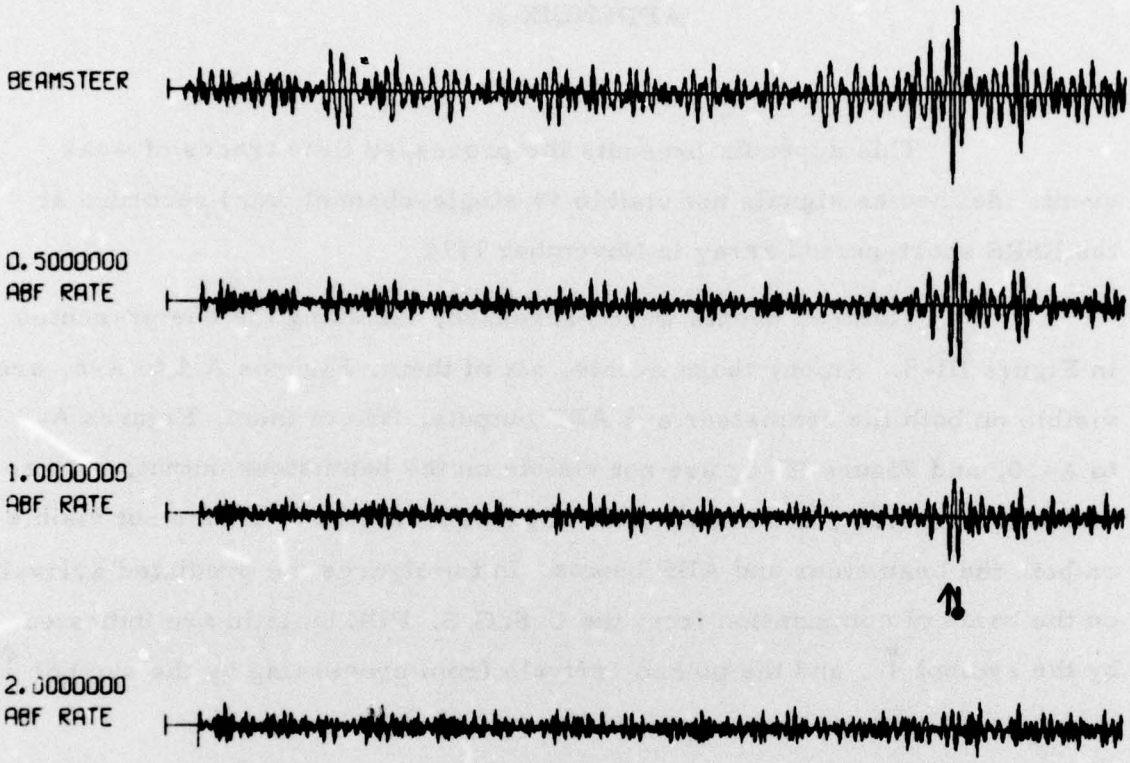


FIGURE A-1

PROCESSED TRACES FOR THE EVENT FROM TURKEY NOVEMBER 5, 1974

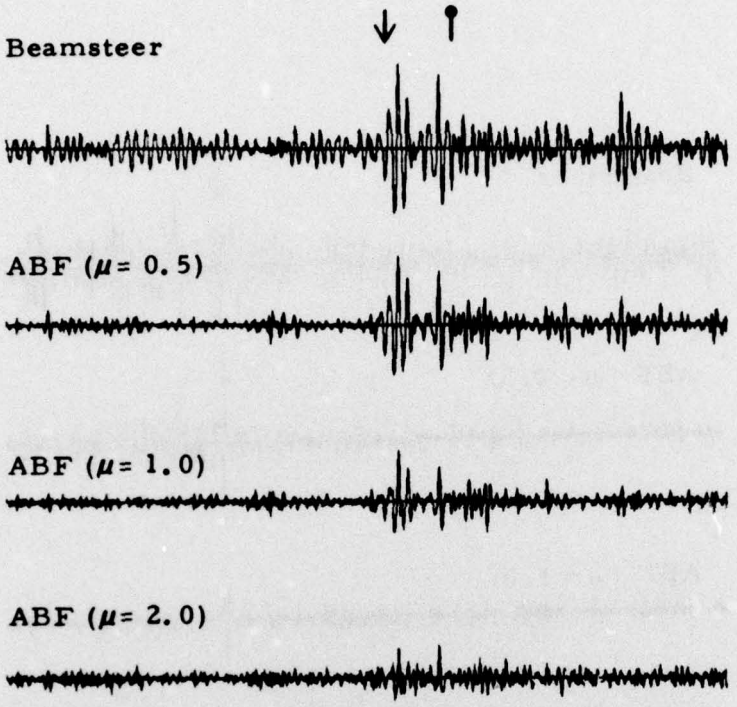


FIGURE A-2

PROCESSED TRACES FOR THE EVENT FROM KASHMIR-INDIA BORDER, NOVEMBER 16, 1974

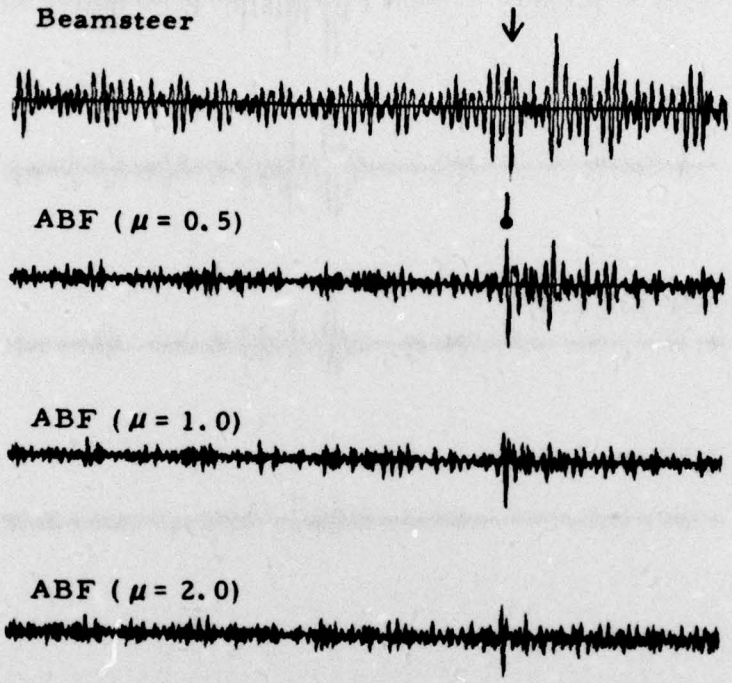


FIGURE A-3

PROCESSED TRACES FOR THE EVENT FROM IRAQ,
NOVEMBER 17, 1974

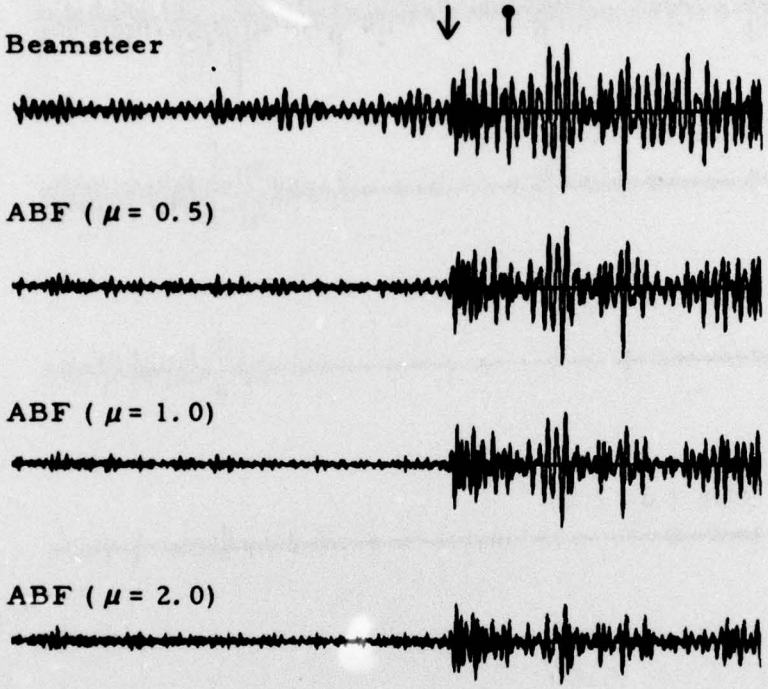


FIGURE A-4

PROCESSED TRACES FOR THE EVENT FROM IRAN
NOVEMBER 22, 1974

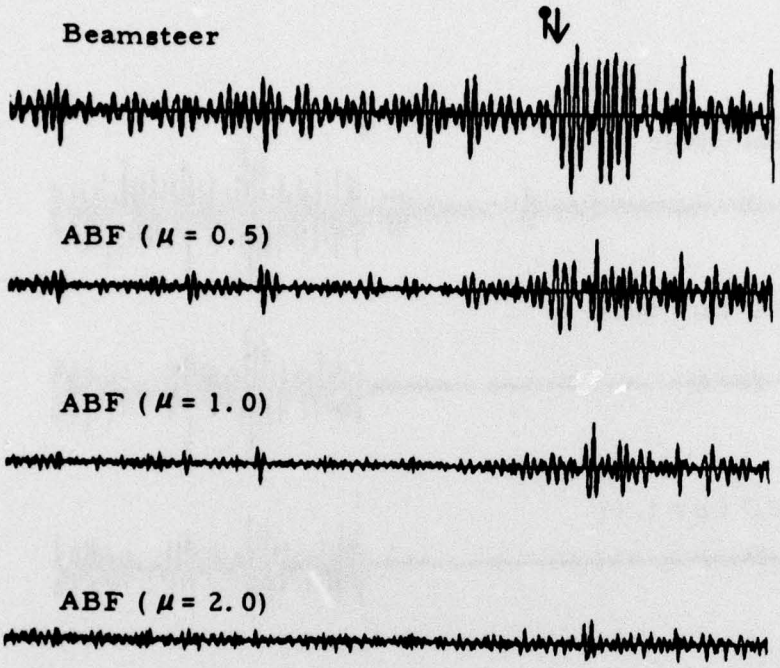


FIGURE A-5

PROCESSED TRACES FOR THE EVENT FROM GREECE - ALBANIA BORDER, NOVEMBER 23, 1974

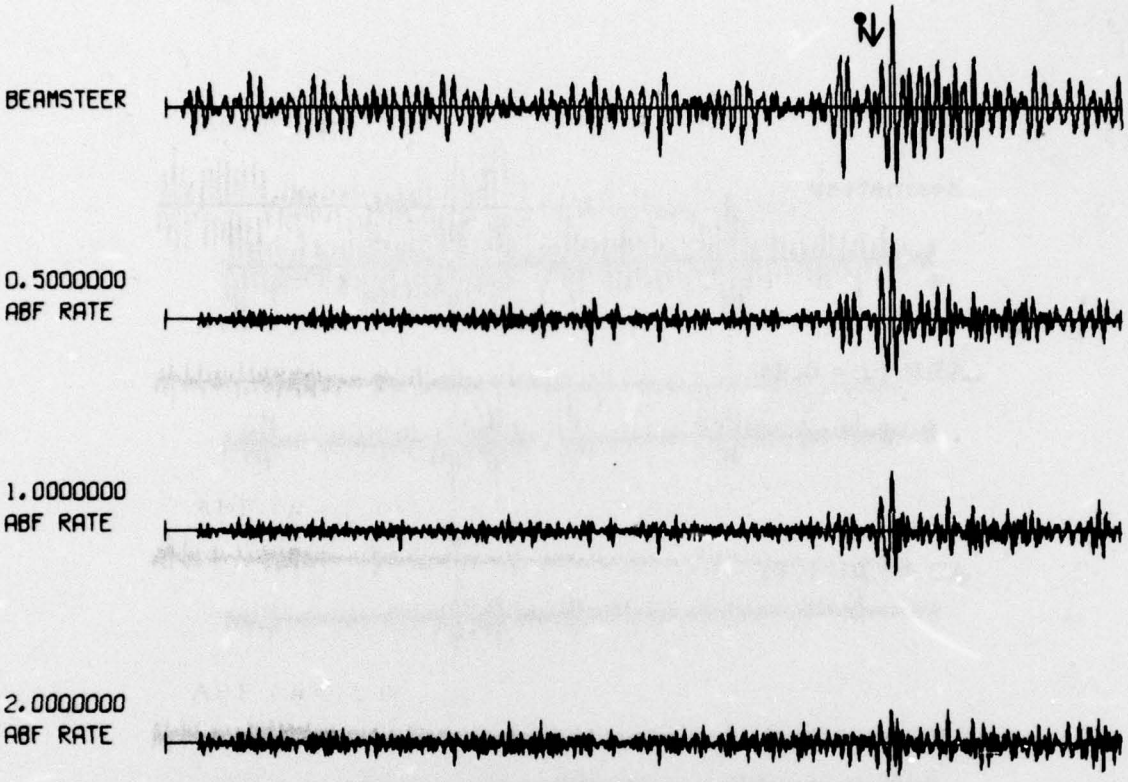


FIGURE A-6

PROCESSED TRACES FOR THE EVENT FROM
SOUTHERN SINKIANG, CHINA, NOVEMBER 28, 1974

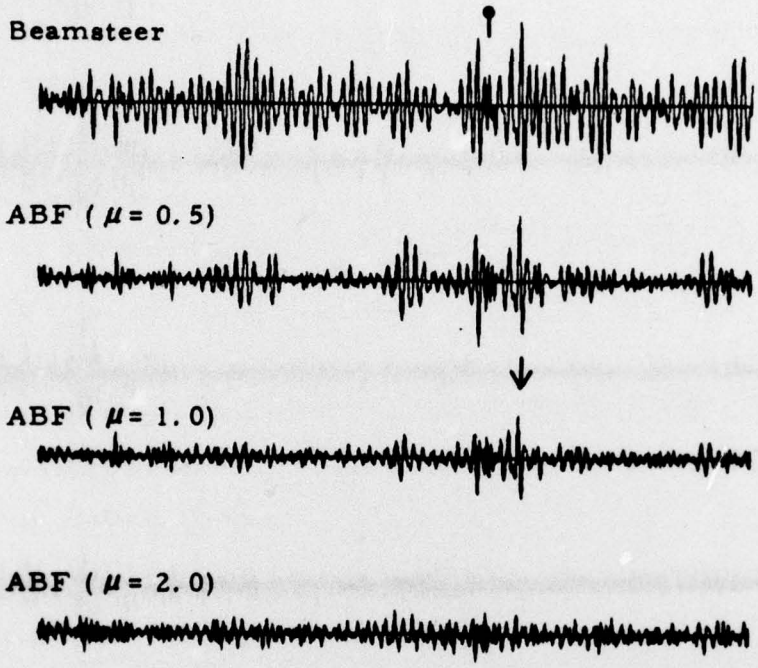


FIGURE A-7

PROCESSED TRACES FOR THE EVENT FROM GREECE
NOVEMBER 14, 1974

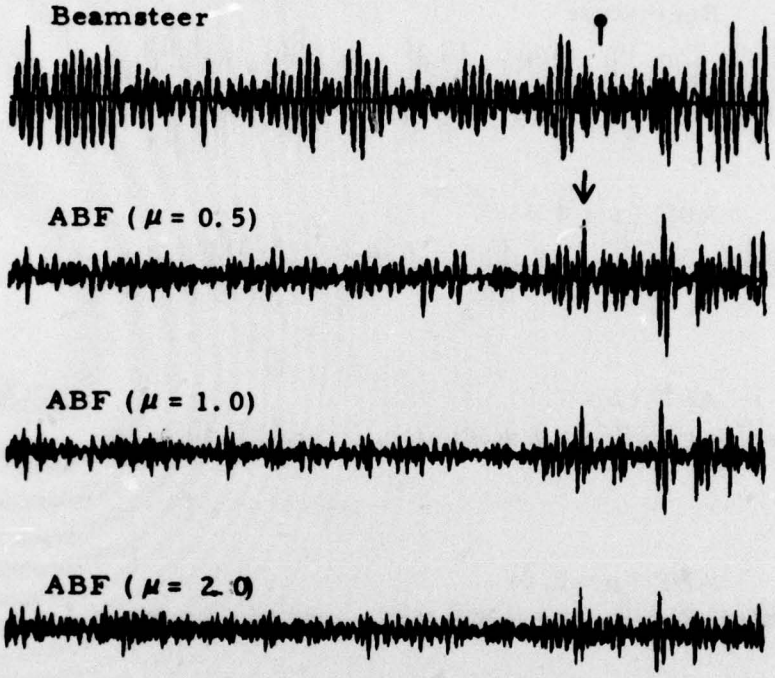


FIGURE A-8

PROCESSED TRACES FOR THE EVENT FROM WESTERN IRAN, NOVEMBER 22, 1974

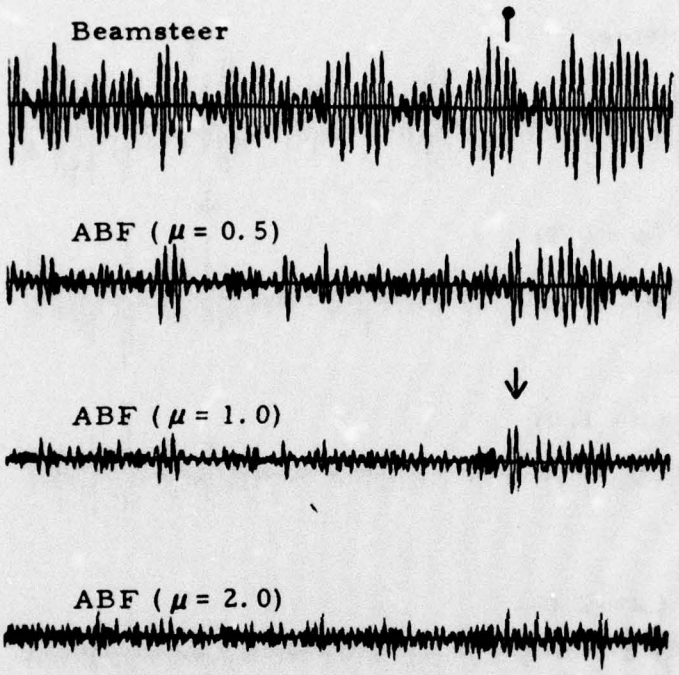


FIGURE A-9

PROCESSED TRACES FOR THE EVENT FROM TURKEY
NOVEMBER 23, 1974

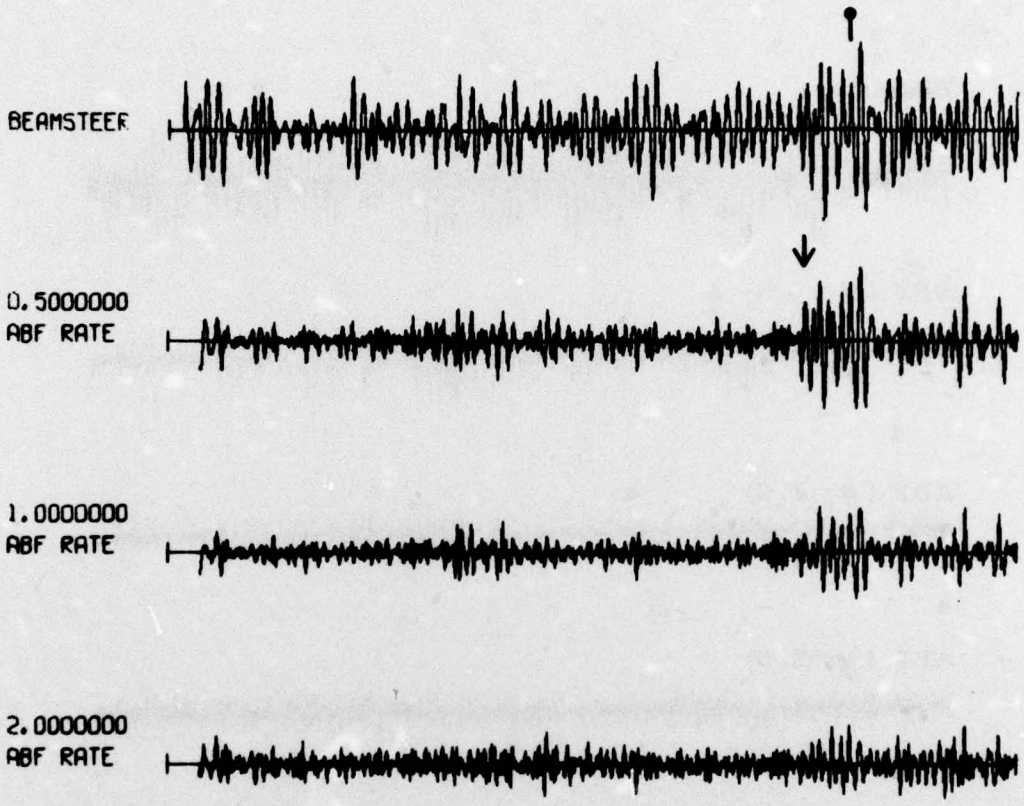


FIGURE A-10

PROCESSED TRACES FOR THE EVENT FROM
SOUTHERN SINKIANG, CHINA, NOVEMBER 25, 1974

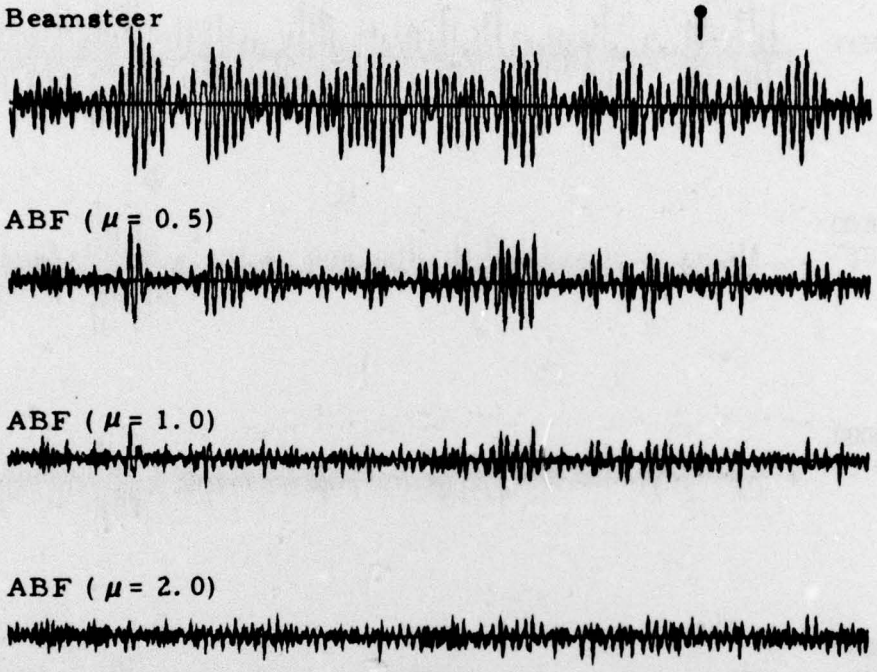


FIGURE A-11

PROCESSED TRACES FOR THE EVENT FROM AFGHANISTAN-USSR BORDER, NOVEMBER 13, 1974

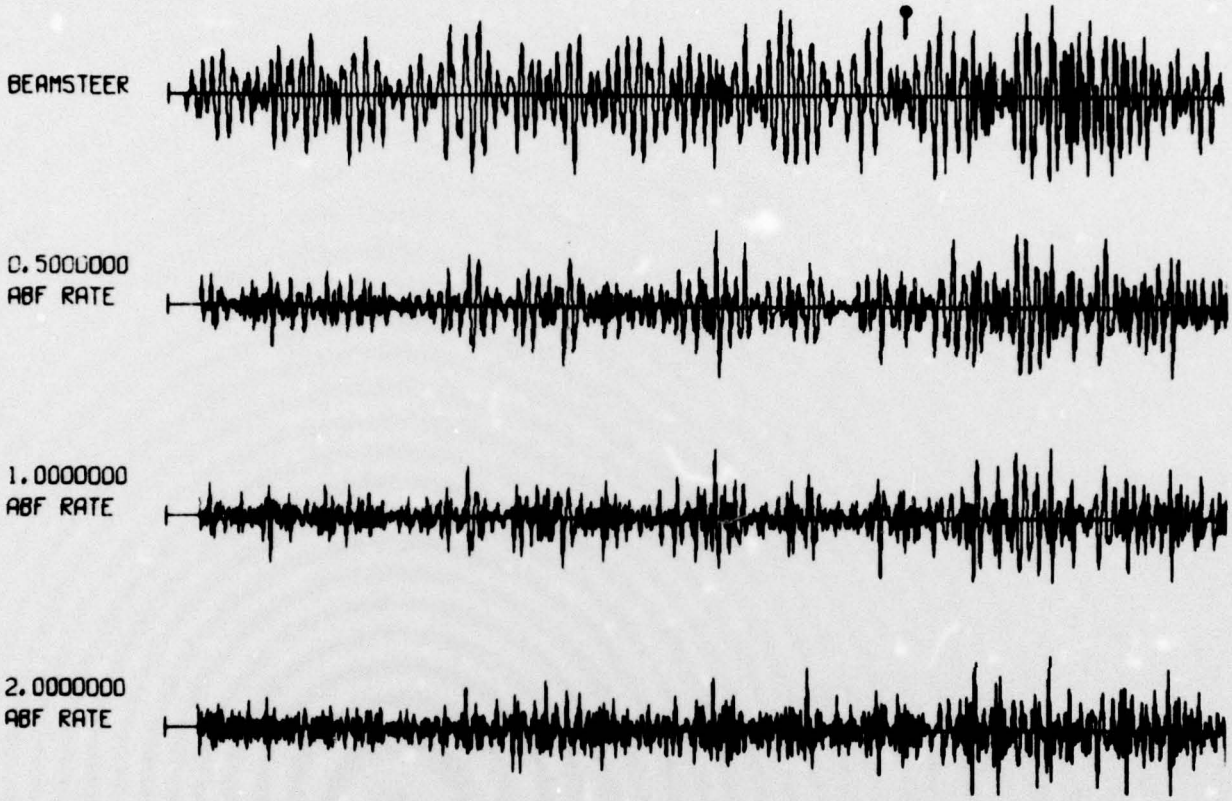


FIGURE A-12

PROCESSED TRACES FOR THE EVENT FROM GREECE,
NOVEMBER 14, 1974